symmetry

MDPI

Article

Nonlocal Elasticity Response of Doubly-Curved Nanoshells

Mohammad Hassan Dindarloo [1], Li Li [2], Rossana Dimitri [3] and Francesco Tornabene [3,*]

[1] Department of Mechanical Engineering, Tarbiat Modares University, Tehran 14115-111, Iran; mhdmhd74@yahoo.com
[2] State Key Lab of Digital Manufacturing Equipment and Technology, School of Mechanical Science and Engineering, Huazhong University of Science and Technology, Wuhan 430074, China; lili_em@hust.edu.cn
[3] Department of Innovation Engineering, University of Salento, 73100 Lecce, Italy; rossana.dimitri@unisalento.it
* Correspondence: francesco.tornabene@unisalento.it

Received: 2 February 2020; Accepted: 10 March 2020; Published: 16 March 2020

Abstract: In this paper, we focus on the bending behavior of isotropic doubly-curved nanoshells based on a high-order shear deformation theory, whose shape functions are selected as an accurate combination of exponential and trigonometric functions instead of the classical polynomial functions. The small-scale effect of the nanostructure is modeled according to the differential law consequent, but is not equivalent to the strain-driven nonlocal integral theory of elasticity equipped with Helmholtz's averaging kernel. The governing equations of the problem are obtained from the Hamilton's principle, whereas the Navier's series are proposed for a closed form solution of the structural problem involving simply-supported nanostructures. The work provides a unified framework for the bending study of both thin and thick symmetric doubly-curved shallow and deep nanoshells, while investigating spherical and cylindrical panels subjected to a point or a sinusoidal loading condition. The effect of several parameters, such as the nonlocal parameter, as well as the mechanical and geometrical properties, is investigated on the bending deflection of isotropic doubly-curved shallow and deep nanoshells. The numerical results from our investigation could be considered as valid benchmarks in the literature for possible further analyses of doubly-curved applications in nanotechnology.

Keywords: doubly-curved nanoshells; high-order shear deformation theory; nonlocal elasticity theory; static analysis

1. Introduction

Doubly-curved shells are three-dimensional structures, commonly used in many engineering applications, such as aerospace structures, airplane vehicles, or big constructions such as stadium cupolas. In their service life, doubly-curved shells are usually affected by different kinds of loading conditions due to their special geometrical shapes. Therefore, the knowledge of their static response is a crucial subject of investigation, especially from an applied design standpoint. The application of adequate numerical models for the bending analysis of doubly-curved shell structures represents a key aspect to be investigated, which is done herein for nanoshell applications. Doubly-curved shells can feature a complex geometry, which makes the exact description of their mathematical problem difficult. Based on the available literature, several theories have been developed to handle the mechanical behavior of complex shell structures, namely, the 3D elasticity [1–3], the Equivalent Single Layer (ESL) theories [4–7], and the Layer Wise (LW) [8–11] theories. In what follows, we propose an ESL model for the static analysis of composite nanoshells with high mechanical magnetic, electronic, and biomedical properties. In this context, classical continuum theories are known to be unable to accurately analyze microstructures or nanostructures and their size effect, whereas the nonlocal theories are more appropriate to account for small scale effects [12–14], together with the physical interactions of atoms and molecules at a microscale or nanoscale.

In recent years, a large number of works has focused on the structural behavior of beams, plates, and shell structures, as briefly reviewed in the following. Ramirez et al. [15] investigated the static analysis of functionally graded (FG) elastic anisotropic plates using a discrete layer approach together with the Ritz method. Merdaci and Belghoul [16] applied a higher-order shear deformation theory (HSDT) with trigonometric shear strain shape functions to study the statics of FG plates with porosities, while assuming the Navier's series to solve the equations of motion. In line with the previous works, Alibeigloo and Nouri [17] studied the statics of FG cylindrical shell with piezoelectric layers by using the differential quadrature method to handle the governing differential equations and boundary conditions. A standard finite element approach was differently applied by Kumar et al. [18] for the static and dynamic analysis of composite cylindrical shells based on the first-order shear deformation theory (FSDT). A nonlinear analysis of the structural response of FG shells was also performed by Frikha and Dammak [19] through the application of discrete double director shell elements. Thin and thick shell theories were proposed alternatively, according to a HSDT, where the material properties were graded throughout the thickness, according to a simple power-law. Moreover, Mantari et al. [20] proposed a novel HSDT to investigate the static and dynamic response of laminated composite and sandwich plates and shells with different geometries. They considered the transverse shear strain field throughout the thickness, along with the tangential stress-free boundary conditions on the shell surface. The governing equations of the problem and the associated boundary conditions were derived by the principle of virtual work whose solution was determined numerically by means of the Navier series.

As far as nanotechnology is concerned, an increased number of works in literature has focused on the nonlocal mechanics of nanostructures [21–26]. More specifically, Sahmani and Aghdam [21] investigated the nonlinear instability of hydrostatic pressurized hybrid nanoshells based on nonlocal elasticity theories, combined to the HSDT. Zeighampour et al. [22] employed a strain gradient theory to investigate the torsional vibrations and static behavior of cylindrical shells, whose equations of motion and non-classical boundary conditions were derived, according to the Hamilton's principle. A further application of the nonlocal elasticity theory can be found in Reference [23] for a parametric study of the axial post-buckling behavior of nanoshells with different nonlocal parameters. Various nonlocal theories have been applied within coupled problems, such as piezoelectric, flexoelectric, or thermo-electro-mechanical shells at different scales both for simple [24–32] or more complex [33–46] geometries.

Based on the available literature, however, limited attention has been paid to the nonlocal mechanical behavior of symmetric doubly-curved deep nanoshells. This is explored for isotropic doubly-curved nanoshells, where we propose a novel nonlocal shear deformation theory, based on a combination of exponential and trigonometric functions. These functions are selected for their higher accuracy compared to the polynomial functions [47]. The small-scale effect of the nanostructure is, thus, modeled, according to a differential law consequent, but not equivalent to the strain-driven nonlocal integral theory of elasticity supplemented with Helmholtz's averaging kernel, whereby the strain-displacement relations for symmetric nanoshells are based on the Reddy's doubly-curved shells theory. The governing equations and boundary conditions are derived by the Hamilton's principle whose theoretical formulation is detailed in Section 2. In Section 3, we propose a Navier-type procedure to solve the problem in a closed-form, whose accuracy is checked against the open literature in Section 4, along with a systematic investigation aimed at studying the influence of nonlocal and geometrical parameters on the deflection response of both shallow and deep doubly-curved isotropic nanoshells. The main conclusive remarks are discussed in the last section, which could be of great interest for scientists and designers for many practical applications.

2. Governing Equations of Doubly-Curved Nanoshells

In this section, we provide a brief overview of the mathematical fundamentals and governing equations of the problem with a special focus on the nonlocal structural response of shallow and deep isotropic doubly-curved nanoshells. The displacement field is modeled based on the combination of exponential, sinusoidal, and cosine strain functions due to their accuracy, as verified in Reference [47]. Figure 1 shows the geometrical scheme of the doubly-curved nanoshell analyzed in this scenario, where h is the thickness of the nanoshell, R_1 and R_2 refer to its curvature radii, a and b stand for its width and length, respectively.

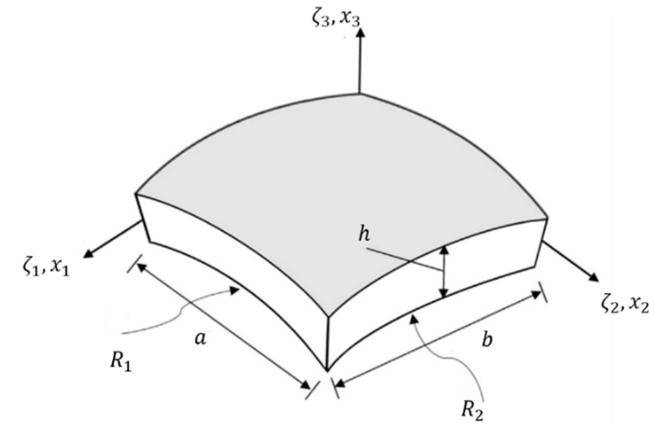

Figure 1. Geometrical scheme of a doubly-curved nanoshell.

Based on the HSDT [20], the displacement field of doubly-curved deep nanoshells are expressed by the equation below.

$$\begin{aligned}
\bar{u}(\xi_1,\xi_2,\xi_3,t) &= \left(1+\frac{\xi_3}{R_1}\right)u(\xi_1,\xi_2,t)+\xi_3\left(y^*\phi_1-\frac{\partial w(\xi_1,\xi_2,t)}{a_1\partial\xi_1}\right)+f(\xi_3)\phi_1(\xi_1,\xi_2,t)\\
\bar{v}(\xi_1,\xi_2,\xi_3,t) &= \left(1+\frac{\xi_3}{R_2}\right)v(\xi_1,\xi_2,t)+\xi_3\left(y^*\phi_2-\frac{\partial w(\xi_1,\xi_2,t)}{a_2\partial\xi_2}\right)+f(\xi_3)\phi_2(\xi_1,\xi_2,t)\\
\bar{w}(\xi_1,\xi_2,\xi_3,t) &= w(\xi_1,\xi_2,t)
\end{aligned} \tag{1}$$

where $\bar{u}(\xi_1,\xi_2,\xi_3,t)$, $\bar{v}(\xi_1,\xi_2,\xi_3,t)$ and $\bar{w}(\xi_1,\xi_2,\xi_3,t)$ are the displacement components along the ξ_1, ξ_2 and ξ_3 directions, respectively. $u(\xi_1,\xi_2,t)$, $v(\xi_1,\xi_2,t)$ and $w(\xi_1,\xi_2,t)$ refer to the displacement field at the mid-surface. $y^*=m\pi/h$ is defined as in Reference [48], whereby the value $m=0.5$ produces the closest response to a 3D elasticity bending solution. Moreover, ϕ_1 and ϕ_2 denote the rotations about ξ_1 and ξ_2 axes, respectively. For an accurate study of the bending response of the doubly-curved deep nanoshells, a combination of the exponential and trigonometric shape functions is proposed within the formulation.

$$f(\xi_3)=\frac{\pi h}{\pi^4+h^4}e^{\left(\frac{h\xi_3}{\pi}\right)}\left(\pi^2\sin\left(\frac{h\xi_3}{\pi}\right)+h^2\cos\left(\frac{h\xi_3}{\pi}\right)\right)-\frac{\pi h^3}{\pi^4+h^4} \tag{2}$$

This is in view of the lower accuracy of polynomial functions [47]. The selected shape function follows the shear deformation distribution throughout the thickness, and satisfies the shear stress-free surface conditions without considering any shear correction factor. Note that, due to the introduction of the shear deformation effect, both thin and thick shell structures are treated in a unified framework.

For a doubly-curved deep shell, the strain-displacement relations can be expressed by the formula below [49].

$$\begin{aligned}
\varepsilon_1 &= \frac{1}{A_1}\left(\frac{\partial \overline{u}}{\partial \xi_1} + \frac{1}{a_2}\frac{\partial a_1}{\partial \xi_2}\overline{v} + \frac{a_1}{R_1}\overline{w}\right) \\
\varepsilon_2 &= \frac{1}{A_2}\left(\frac{\partial \overline{v}}{\partial \xi_2} + \frac{1}{a_1}\frac{\partial a_2}{\partial \xi_1}\overline{u} + \frac{a_2}{R_2}\overline{w}\right) \\
\varepsilon_6 &= \frac{A_2}{A_1}\frac{\partial}{\partial \xi_1}\left(\frac{\overline{v}}{A_2}\right) + \frac{A_1}{A_2}\frac{\partial}{\partial \xi_2}\left(\frac{\overline{u}}{A_1}\right) \\
\varepsilon_4 &= \frac{1}{A_2}\frac{\partial \overline{w}}{\partial \xi_2} + A_2\frac{\partial}{\partial \xi_3}\left(\frac{\overline{v}}{A_2}\right) \\
\varepsilon_5 &= \frac{1}{A_1}\frac{\partial \overline{w}}{\partial \xi_1} + A_1\frac{\partial}{\partial \xi_3}\left(\frac{\overline{u}}{A_1}\right)
\end{aligned} \tag{3}$$

where

$$A_1 = \left(1 + \frac{\xi_3}{R_1}\right)a_1;\ \ A_2 = \left(1 + \frac{\xi_3}{R_2}\right)a_2 \tag{4}$$

a_1 and a_2 representing the tangent vectors along the ξ_1 and ξ_2 directions, respectively, and $\varepsilon_i = (i = 1, 2, \ldots, 6)$ are strain components.

The doubly-curved shallow nanoshell represents a limit case when it is possible to neglect ξ_3 due to its small dimension compared to the curvature radii, i.e.,

$$\begin{aligned}
&\frac{\xi_3}{R_1} \to 0 \Rightarrow 1 + \frac{\xi_3}{R_1} \to 1 \Rightarrow A_1 = a_1 \\
&\frac{\xi_3}{R_2} \to 0 \Rightarrow 1 + \frac{\xi_3}{R_2} \to 1 \Rightarrow A_2 = a_2
\end{aligned} \tag{5}$$

By substituting Equation (1) into Equation (3), we get the following relations.

$$
\begin{aligned}
\varepsilon_1 &= \frac{1}{A_1}\left(\begin{array}{l}\left(1+\frac{\xi_3}{R_1}\right)\frac{\partial u}{\partial \xi_1}+\xi_3\left(y^*\frac{\partial \phi_1}{\partial \xi_1}-\frac{\partial^2 w}{a_1\partial \xi_1{}^2}\right)+f\left(\xi_3\right)\frac{\partial \phi_1}{\partial \xi_1}+ \\ +\frac{1}{a_2}\frac{\partial a_1}{\partial \xi_2}\left(\left(1+\frac{\xi_3}{R_2}\right)v+\xi_3\left(y^*\phi_2-\frac{\partial w}{a_2\partial \xi_2}\right)+f\left(\xi_3\right)\phi_2\right)+\frac{a_1}{R_1}w\end{array}\right) \\
\varepsilon_2 &= \frac{1}{A_2}\left(\begin{array}{l}\left(1+\frac{\xi_3}{R_2}\right)\frac{\partial v}{\partial \xi_2}+\xi_3\left(y^*\frac{\partial \phi_2}{\partial \xi_2}-\frac{\partial^2 w}{a_2\partial \xi_2{}^2}\right)+f\left(\xi_3\right)\frac{\partial \phi_2}{\partial \xi_2}+ \\ +\frac{1}{a_1}\frac{\partial a_2}{\partial \xi_1}\left(\left(1+\frac{\xi_3}{R_1}\right)u+\xi_3\left(y^*\phi_1-\frac{\partial w}{a_1\partial \xi_1}\right)+f\left(\xi_3\right)\phi_1\right)+\frac{a_2}{R_2}w\end{array}\right) \\
\varepsilon_6 &= \frac{1}{A_1}\left(\left(1+\frac{\xi_3}{R_2}\right)\frac{\partial v}{\partial \xi_1}+\xi_3\left(y^*\frac{\partial \phi_2}{\partial \xi_1}-\frac{\partial^2 w}{a_2\partial \xi_1\partial \xi_2}\right)+f\left(\xi_3\right)\frac{\partial \phi_2}{\partial \xi_1}\right)+ \\
&\quad +\frac{1}{A_2}\left(\left(1+\frac{\xi_3}{R_1}\right)\frac{\partial u}{\partial \xi_2}+\xi_3\left(y^*\frac{\partial \phi_1}{\partial \xi_2}-\frac{\partial^2 w}{a_1\partial \xi_1\partial \xi_2}\right)+f\left(\xi_3\right)\frac{\partial \phi_1}{\partial \xi_2}\right) \\
\varepsilon_4 &= \frac{1}{A_2}\frac{\partial w}{\partial \xi_2}+\frac{1}{R_2}v+y^*\phi_2-\frac{\partial w}{a_2\partial \xi_2}+\frac{df\left(\xi_3\right)}{d\xi_3}\phi_2 \\
\varepsilon_5 &= \frac{1}{A_1}\frac{\partial w}{\partial \xi_1}+\frac{1}{R_1}u+y^*\phi_1-\frac{\partial w}{a_1\partial \xi_1}+\frac{df\left(\xi_3\right)}{d\xi_3}\phi_1
\end{aligned}
\tag{6}
$$

The size effect of doubly-curved nanoshells starts considering the strain-driven gradient model by Eringen [13] to include possible nonlocal long-range interactions, which is also discussed for beam applications in References [50–53]. Thus, the stress-strain relations for both thin and thick isotropic nanoshells, accounting for small effects, are expressed by the equation below

$$
\left(1-\mu^2\nabla^2\right)\begin{Bmatrix}\sigma_1\\ \sigma_2\\ \sigma_6\\ \sigma_4\\ \sigma_5\end{Bmatrix}=\begin{bmatrix}Q_{11} & Q_{12} & 0 & 0 & 0\\ Q_{12} & Q_{22} & 0 & 0 & 0\\ 0 & 0 & Q_{66} & 0 & 0\\ 0 & 0 & 0 & Q_{44} & 0\\ 0 & 0 & 0 & 0 & Q_{55}\end{bmatrix}\begin{Bmatrix}\varepsilon_1\\ \varepsilon_2\\ \varepsilon_6\\ \varepsilon_4\\ \varepsilon_5\end{Bmatrix}
\tag{7}
$$

where

$$
Q_{11}=Q_{22}=\frac{E}{1-\nu^2} \quad , \quad Q_{12}=\frac{\nu E}{1-\nu^2} \quad , \quad Q_{44}=Q_{55}=Q_{66}=G
\tag{8}
$$

μ is the nonlocal parameter, E and G stand for the Young's modulus and shear modulus of the nanoshell, respectively, and ν is the Poisson's ratio. By combining Equations (6) and (7), we get the following.

$$
\begin{aligned}
&\sigma_1-\mu^2\left(\frac{\partial^2\sigma_1}{a_1^2\partial\xi_1^2}+\frac{\partial^2\sigma_1}{a_2^2\partial\xi_2^2}\right)=\frac{Q_{11}}{A_1}\left(\begin{aligned}&\left(1+\frac{\xi_3}{R_1}\right)\frac{\partial u}{\partial\xi_1}+\xi_3\left(y^*\frac{\partial\phi_1}{\partial\xi_1}-\frac{\partial^2 w}{a_1\partial\xi_1{}^2}\right)+f\left(\xi_3\right)\frac{\partial\phi_1}{\partial\xi_1}+\\&+\frac{1}{a_2}\frac{\partial a_1}{\partial\xi_2}\left(\left(1+\frac{\xi_3}{R_2}\right)v+\xi_3\left(y^*\phi_2-\frac{\partial w}{a_2\partial\xi_2}\right)+f\left(\xi_3\right)\phi_2\right)+\frac{a_1}{R_1}w\end{aligned}\right)\\
&+\frac{Q_{12}}{A_2}\left(\begin{aligned}&\left(1+\frac{\xi_3}{R_2}\right)\frac{\partial v}{\partial\xi_2}+\xi_3\left(y^*\frac{\partial\phi_2}{\partial\xi_2}-\frac{\partial^2 w}{a_2\partial\xi_2{}^2}\right)+f\left(\xi_3\right)\frac{\partial\phi_2}{\partial\xi_2}+\\&+\frac{1}{a_1}\frac{\partial a_2}{\partial\xi_1}\left(\left(1+\frac{\xi_3}{R_1}\right)u+\xi_3\left(y^*\phi_1-\frac{\partial w}{a_1\partial\xi_1}\right)+f\left(\xi_3\right)\phi_1\right)+\frac{a_2}{R_2}w\end{aligned}\right)\\
&\sigma_2-\mu^2\left(\frac{\partial^2\sigma_2}{a_1^2\partial\xi_1^2}+\frac{\partial^2\sigma_2}{a_2^2\partial\xi_2^2}\right)=\frac{Q_{12}}{A_1}\left(\begin{aligned}&\left(1+\frac{\xi_3}{R_1}\right)\frac{\partial u}{\partial\xi_1}+\xi_3\left(y^*\frac{\partial\phi_1}{\partial\xi_1}-\frac{\partial^2 w}{a_1\partial\xi_1{}^2}\right)+f\left(\xi_3\right)\frac{\partial\phi_1}{\partial\xi_1}+\\&+\frac{1}{a_2}\frac{\partial a_1}{\partial\xi_2}\left(\left(1+\frac{\xi_3}{R_2}\right)v+\xi_3\left(y^*\phi_2-\frac{\partial w}{a_2\partial\xi_2}\right)+f\left(\xi_3\right)\phi_2\right)+\frac{a_1}{R_1}w\end{aligned}\right)\\
&+\frac{Q_{22}}{A_2}\left(\begin{aligned}&\left(1+\frac{\xi_3}{R_2}\right)\frac{\partial v}{\partial\xi_2}+\xi_3\left(y^*\frac{\partial\phi_2}{\partial\xi_2}-\frac{\partial^2 w}{a_2\partial\xi_2{}^2}\right)+f\left(\xi_3\right)\frac{\partial\phi_2}{\partial\xi_2}+\\&+\frac{1}{a_1}\frac{\partial a_2}{\partial\xi_1}\left(\left(1+\frac{\xi_3}{R_1}\right)u+\xi_3\left(y^*\phi_1-\frac{\partial w}{a_1\partial\xi_1}\right)+f\left(\xi_3\right)\phi_1\right)+\frac{a_2}{R_2}w\end{aligned}\right)\\
&\sigma_6-\mu^2\left(\frac{\partial^2\sigma_6}{a_1^2\partial\xi_1^2}+\frac{\partial^2\sigma_6}{a_2^2\partial\xi_2^2}\right)=\frac{Q_{66}}{A_1}\left(\left(1+\frac{\xi_3}{R_2}\right)\frac{\partial v}{\partial\xi_1}+\xi_3\left(y^*\frac{\partial\phi_2}{\partial\xi_1}-\frac{\partial^2 w}{a_2\partial\xi_1\partial\xi_2}\right)+f\left(\xi_3\right)\frac{\partial\phi_2}{\partial\xi_1}\right)+\\
&+\frac{Q_{66}}{A_2}\left(\left(1+\frac{\xi_3}{R_1}\right)\frac{\partial u}{\partial\xi_2}+\xi_3\left(y^*\frac{\partial\phi_1}{\partial\xi_2}-\frac{\partial^2 w}{a_1\partial\xi_1\partial\xi_2}\right)+f\left(\xi_3\right)\frac{\partial\phi_1}{\partial\xi_2}\right)\\
&\sigma_4-\mu^2\left(\frac{\partial^2\sigma_4}{a_1^2\partial\xi_1^2}+\frac{\partial^2\sigma_4}{a_2^2\partial\xi_2^2}\right)=Q_{44}\left(\frac{1}{A_2}\frac{\partial w}{\partial\xi_2}+\frac{1}{R_2}v+y^*\phi_2-\frac{\partial w}{a_2\partial\xi_2}+\frac{df\left(\xi_3\right)}{d\xi_3}\phi_2\right)\\
&\sigma_5-\mu^2\left(\frac{\partial^2\sigma_5}{a_1^2\partial\xi_1^2}+\frac{\partial^2\sigma_5}{a_2^2\partial\xi_2^2}\right)=Q_{55}\left(\frac{1}{A_1}\frac{\partial w}{\partial\xi_1}+\frac{1}{R_1}u+y^*\phi_1-\frac{\partial w}{a_1\partial\xi_1}+\frac{df\left(\xi_3\right)}{d\xi_3}\phi_1\right)
\end{aligned}
\tag{9}
$$

The equations of motion are derived from the Hamilton's principle, defined in a variational form as follows.

$$
\int_{t_1}^{t_2}\left(\delta U-\delta T+\delta W\right)\mathrm{d}t=0 \tag{10}
$$

where δU and δT denote the variation of the strain energy and kinetic energy, respectively, δW is the variation of the external work. Equation (10) can be written in an extended version as follows

$$
\int_{t_1}^{t_2}\int_0^a\int_0^b\int_{-\frac{h}{2}}^{\frac{h}{2}}\left(\sigma_1\delta\varepsilon_1+\sigma_2\delta\varepsilon_2+\sigma_6\delta\varepsilon_6+\sigma_4\delta\varepsilon_4+\sigma_5\delta\varepsilon_5\right)\mathrm{a}_1\mathrm{a}_2\mathrm{a}_3\mathrm{d}\xi_1\mathrm{d}\xi_2\mathrm{d}\xi_3\mathrm{d}t-\int_{-\frac{h}{2}}^{\frac{h}{2}}q\delta w\mathrm{a}_1\mathrm{a}_2\mathrm{a}_3\mathrm{d}\xi_1\mathrm{d}\xi_2\mathrm{d}\xi_3\mathrm{d}t=0 \tag{11}
$$

where q is the transverse load. The variation of the strain energy can be defined in terms of axial, shear, and moment resultants, as follows

$$\begin{aligned}
\delta U &= \int_0^a \int_0^b \int_{-\frac{h}{2}}^{\frac{h}{2}} \left(\sigma_1 \delta\varepsilon_1 + \sigma_2 \delta\varepsilon_2 + \sigma_6 \delta\varepsilon_6 + \sigma_4 \delta\varepsilon_4 + \sigma_5 \delta\varepsilon_5\right) \mathrm{a}_1 \mathrm{a}_2 \mathrm{a}_3 \mathrm{d}\xi_1 \mathrm{d}\xi_2 \mathrm{d}\xi_3 = \\
&= \int_0^a \int_0^b \left[\frac{N_1}{A_1} \left(\left(1 + \frac{\xi_3}{R_1}\right) \frac{\partial \delta u}{\partial \xi_1} + \frac{1}{a_2} \frac{\partial a_1}{\partial \xi_2} \left(1 + \frac{\xi_3}{R_2}\right) \delta v + \frac{a_1}{R_1} \delta w \right) + \frac{M_1}{A_1} \left(y^* \frac{\partial \delta \phi_1}{\partial \xi_1} - \frac{\partial^2 \delta w}{a_1 \partial \xi_1^{\,2}} \right) + \frac{P_1}{A_1} \left(\frac{\partial \delta \phi_1}{\partial \xi_1} \right) \right] \mathrm{a}_1 \mathrm{a}_2 \mathrm{d}\xi_1 \mathrm{d}\xi_2 + \\
&+ \int_0^a \int_0^b \left[\frac{N_2}{A_2} \left(\left(1 + \frac{\xi_3}{R_2}\right) \frac{\partial \delta v}{\partial \xi_2} + \frac{1}{a_1} \frac{\partial a_2}{\partial \xi_1} \left(1 + \frac{\xi_3}{R_1}\right) \delta u + \frac{a_2}{R_2} \delta w \right) + \frac{M_2}{A_2} \left(y^* \frac{\partial \delta \phi_2}{\partial \xi_2} - \frac{\partial^2 \delta w}{a_2 \partial \xi_2^{\,2}} \right) + \frac{P_2}{A_2} \left(\frac{\partial \delta \phi_2}{\partial \xi_2} \right) \right] \mathrm{a}_1 \mathrm{a}_2 \mathrm{d}\xi_1 \mathrm{d}\xi_2 + \\
&+ \int_0^a \int_0^b \left[\begin{array}{l} N_6 \left(\frac{1}{A_1} \left(1 + \frac{\xi_3}{R_2}\right) \frac{\partial \delta v}{\partial \xi_1} + \frac{1}{A_2} \left(1 + \frac{\xi_3}{R_1}\right) \frac{\partial \delta u}{\partial \xi_2} \right) + \\ + M_6 \left(\frac{1}{A_1} \left(y^* \frac{\partial \delta \phi_2}{\partial \xi_1} - \frac{\partial^2 \delta w}{a_2 \partial \xi_1 \partial \xi_2} \right) + \frac{1}{A_2} \left(y^* \frac{\partial \delta \phi_1}{\partial \xi_2} - \frac{\partial^2 \delta w}{a_1 \partial \xi_1 \partial \xi_2} \right) \right) + P_6 \left(\frac{1}{A_1} \frac{\partial \delta \phi_2}{\partial \xi_1} + \frac{1}{A_2} \frac{\partial \delta \phi_1}{\partial \xi_2} \right) \end{array} \right] \mathrm{a}_1 \mathrm{a}_2 \mathrm{d}\xi_1 \mathrm{d}\xi_2 + \\
&+ \int_0^a \int_0^b \left[Q_2 \left(\frac{1}{A_2} \frac{\partial \delta w}{\partial \xi_2} + \frac{1}{R_2} \delta v + y^* \delta \phi_2 - \frac{\partial \delta w}{a_2 \partial \xi_2} \right) + K_2 \delta \phi_2 \right] \mathrm{a}_1 \mathrm{a}_2 \mathrm{d}\xi_1 \mathrm{d}\xi_2 + \\
&+ \int_0^a \int_0^b \left[Q_1 \left(\frac{1}{A_1} \frac{\partial \delta w}{\partial \xi_1} + \frac{1}{R_1} \delta u + y^* \delta \phi_1 - \frac{\partial \delta w}{a_1 \partial \xi_1} \right) + K_1 \delta \phi_1 \right] \mathrm{a}_1 \mathrm{a}_2 \mathrm{d}\xi_1 \mathrm{d}\xi_2
\end{aligned} \tag{12}$$

where

$$\begin{aligned}
\left(N_i, M_i, P_i\right) &= \int_{-\frac{h}{2}}^{\frac{h}{2}} \sigma_i \left(1, \xi_3, \mathrm{f}(\xi)\right) d\xi_3 \qquad (i = 1,2,6) \\
\left(Q_1, \mathrm{K}_1\right) &= \int_{-\frac{h}{2}}^{\frac{h}{2}} \sigma_5 \left(1, \frac{df}{d\xi}\right) d\xi_3 \\
\left(Q_2, \mathrm{K}_2\right) &= \int_{-\frac{h}{2}}^{\frac{h}{2}} \sigma_4 \left(1, \frac{df}{d\xi}\right) d\xi_3
\end{aligned} \tag{13}$$

By substituting Equation (12) in Equation (11), the static equations for the isotropic doubly-curved nanoshells can be derived by the formula below

$$\begin{aligned}
&\delta u: \frac{\partial}{\partial \xi_1} \left(\frac{N_1}{A_1} \left(1 + \frac{\xi_3}{R_1}\right) \right) + \frac{\partial}{\partial \xi_2} \left(\frac{N_6}{A_2} \left(1 + \frac{\xi_3}{R_1}\right) \right) - \frac{N_2}{A_2} \left(\frac{1}{a_1} \frac{\partial a_2}{\partial \xi_1} \left(1 + \frac{\xi_3}{R_1}\right) \right) - \frac{Q_1}{R_1} = 0 \\
&\delta v: \frac{\partial}{\partial \xi_2} \left(\frac{N_2}{A_2} \left(1 + \frac{\xi_3}{R_2}\right) \right) + \frac{\partial}{\partial \xi_1} \left(\frac{N_6}{A_1} \left(1 + \frac{\xi_3}{R_1}\right) \right) - \frac{N_1}{A_1} \left(\frac{1}{a_2} \frac{\partial a_1}{\partial \xi_2} \left(1 + \frac{\xi_3}{R_2}\right) \right) - \frac{Q_2}{R_2} = 0 \\
&\delta w: \frac{\partial^2}{\partial \xi_1^{\,2}} \left(\frac{M_1}{A_1 a_1} \right) + \frac{\partial^2}{\partial \xi_2^{\,2}} \left(\frac{M_2}{A_2 a_2} \right) + \frac{\partial^2}{\partial \xi_1 \partial \xi_2} \left(\frac{M_6}{A_1 a_2} \right) + \frac{\partial^2}{\partial \xi_1 \partial \xi_2} \left(\frac{M_6}{A_2 a_1} \right) + \frac{\partial}{\partial \xi_2} \left(\frac{Q_2}{A_2} \right) + \frac{\partial}{\partial \xi_1} \left(\frac{Q_1}{A_1} \right) + \\
&- \frac{\partial}{\partial \xi_2} \left(\frac{Q_2}{a_2} \right) - \frac{\partial}{\partial \xi_1} \left(\frac{Q_1}{a_1} \right) - \frac{a_1}{R_1} \frac{N_1}{A_1} - \frac{a_2}{R_2} \frac{N_2}{A_2} = -q \\
&\delta \phi_1: \frac{\partial}{\partial \xi_1} \left(\frac{M_1 y^*}{A_1} \right) + \frac{\partial}{\partial \xi_2} \left(\frac{M_6 y^*}{A_2} \right) + \frac{\partial}{\partial \xi_1} \left(\frac{P_1}{A_1} \right) + \frac{\partial}{\partial \xi_2} \left(\frac{P_6}{A_2} \right) - Q_1 y^* - K_1 = 0 \\
&\delta \phi_2: \frac{\partial}{\partial \xi_2} \left(\frac{M_2 y^*}{A_2} \right) + \frac{\partial}{\partial \xi_1} \left(\frac{M_6 y^*}{A_1} \right) + \frac{\partial}{\partial \xi_2} \left(\frac{P_2}{A_2} \right) + \frac{\partial}{\partial \xi_1} \left(\frac{P_6}{A_1} \right) - Q_2 y^* - K_2 = 0
\end{aligned} \tag{14}$$

By substituting Equations (9) and (13) into Equation (14), the equations of motion for deep spherical panels can be rewritten in terms of displacement components, as shown below

$$
\begin{aligned}
&\frac{A_{11}}{R_1}\frac{\partial w}{a_1\,\partial\xi_1}+A_{13}\frac{\partial^2 u}{\partial\xi^{2}{}_{1}}+A_{16}\left(y^*\frac{\partial^2\phi_1}{a_1^2\partial\xi^{2}{}_{1}}-\frac{\partial^3 w}{a_1^3\partial\xi_1^{3}}\right)+A_{17}\frac{\partial^2\phi_1}{a_1^2\partial\xi^{2}{}_{1}}+\frac{B_{11}}{R_2}\frac{\partial w}{a_1\,\partial\xi_1}+\\
&+B_{15}\frac{\partial^2 v}{a_1\,a_2\partial\xi_1\partial\xi_2}+B_{16}\left(y^*\frac{\partial^2\phi_2}{a_1\,a_2\partial\xi_1\partial\xi_2}-\frac{\partial^3 w}{a_1a_2^2\partial\xi_1\partial\xi_2^{\,2}}\right)+B_{17}\frac{\partial^2\phi_2}{a_1\,a_2\partial\xi_1\partial\xi_2}+\\
&+D_{13}\frac{\partial^2 u}{a_2^2\partial\xi^{2}{}_{2}}+D_{15}\frac{\partial^2 v}{a_1\,a_2\partial\xi_1\partial\xi_2}+D_{16}\left(y^*\left(\frac{\partial^2\phi_1}{\partial\xi^{2}{}_{2}}+\frac{\partial^2\phi_2}{a_1\,a_2\partial\xi_1\partial\xi_2}\right)-\frac{2\partial^3 w}{a_1a_2^2\partial\xi_1\partial\xi^{2}{}_{2}}\right)+\\
&+D_{17}\left(\frac{\partial^2\phi_2}{a_1\,a_2\partial\xi_1\partial\xi_2}+\frac{\partial^2\phi_1}{a_2^2\partial\xi^{2}{}_{2}}\right)-\frac{G_{11}}{R_1}\left(\frac{\partial w}{a_1\partial\xi_1}+\frac{1}{R_1}u+y^*\phi_1-\frac{\partial w}{a_1\partial\xi_1}\right)-\frac{1}{R_1}G_{13}\phi_1=0
\end{aligned}
\tag{15a}
$$

$$
\begin{aligned}
&\frac{B_{12}}{R_1}\frac{\partial w}{a_2\partial\xi_2}+B_{15}\frac{\partial^2 u}{a_1a_2\partial\xi_1\partial\xi_2}+B_{18}\left(y^*\frac{\partial^2\phi_1}{a_1a_2\partial\xi_1\partial\xi_2}-\frac{\partial^3 w}{a_1^2a_2\partial\xi_1^{\,2}\partial\xi_2}\right)+B_{19}\frac{\partial^2\phi_1}{a_1a_2\partial\xi_1\partial\xi_2}+\\
&+\frac{C_{12}}{R_2}\frac{\partial w}{a_2\partial\xi_2}+C_{14}\frac{\partial^2 v}{a_2^2\partial\xi^{2}{}_{2}}+C_{18}\left(y^*\frac{\partial^2\phi_2}{a_2^2\partial\xi^{2}{}_{2}}-\frac{\partial^3 w}{a_2^3\partial\xi_2^{\,3}}\right)+C_{19}\frac{\partial^2\phi_2}{a_2^2\partial\xi^{2}{}_{2}}+\\
&+D_{13}\frac{\partial^2 u}{a_1a_2\partial\xi_2\partial\xi_1}+D_{15}\frac{\partial^2 v}{a_1^2\partial\xi_1^{\,2}}+D_{16}\left(y^*\left(\frac{\partial^2\phi_2}{a_1^2\partial\xi^{2}{}_{1}}+\frac{\partial^2\phi_1}{a_1a_2\partial\xi_2\partial\xi_1}\right)-\frac{2\partial^3 w}{a_1^2a_2\partial\xi_1^{\,2}\partial\xi_2}\right)+\\
&+D_{17}\left(\frac{\partial^2\phi_1}{a_1a_2\partial\xi_1\partial\xi_2}+\frac{\partial^2\phi_2}{a_1^2\partial\xi^{2}{}_{1}}\right)-\frac{F_{11}}{R_2}\left(\frac{\partial w}{a_2\partial\xi_2}+\frac{1}{R_2}v+y^*\phi_2-\frac{\partial w}{a_2\partial\xi_2}\right)-\frac{1}{R_2}F_{13}\phi_2=0
\end{aligned}
\tag{15b}
$$

$$
\begin{aligned}
&-\frac{A_4}{R_1^{\,2}}w-\frac{A_5}{R_1}\left(y^*\frac{\partial\phi_1}{a_1\,\partial\xi_1}-\frac{2\partial^2 w}{a_1^2\partial\xi_1^{\,2}}\right)+A_6\left(y^*\frac{\partial^3\phi_1}{a_1^3\partial\xi^{3}{}_{1}}-\frac{\partial^4 w}{a_1^4\partial\xi_1^{\,4}}\right)-\frac{A_8}{R_1}\frac{\partial\phi_1}{a_1\,\partial\xi_1}+A_9\frac{\partial^3\phi_1}{a_1^3\partial\xi^{3}{}_{1}}+\\
&-\frac{A_{11}}{R_1}\frac{\partial u}{a_1\,\partial\xi_1}+A_{16}\frac{\partial^3 u}{a_1^3\partial\xi^{3}{}_{1}}-\frac{2B_4}{R_1R_2}w-B_5\left(\frac{1}{R_1}\left(y^*\frac{\partial\phi_2}{a_2\partial\xi_2}-\frac{2\partial^2 w}{a_2^2\partial\xi_2^{\,2}}\right)+\frac{1}{R_2}\left(y^*\frac{\partial\phi_1}{a_1\,\partial\xi_1}-\frac{2\partial^2 w}{a_1^2\partial\xi_1^{\,2}}\right)\right)+\\
&+B_6\left(y^*\left(\frac{\partial^3\phi_2}{a_1^2a_2\partial\xi^{2}{}_{1}\partial\xi_2}+\frac{\partial^3\phi_1}{a_2^2a_1\partial\xi_2^{\,2}\partial\xi_1}\right)-\frac{2\partial^4 w}{a_1^2a_2^2\partial\xi^{2}{}_{1}\partial\xi_2^{\,2}}\right)-B_8\left(\frac{1}{R_1}\frac{\partial\phi_2}{a_2\partial\xi_2}+\frac{1}{R_2}\frac{\partial\phi_1}{a_1\,\partial\xi_1}\right)+\\
&+B_9\left(\frac{\partial^3\phi_1}{a_2^2a_1\partial\xi_2^{\,2}\partial\xi_1}+\frac{\partial^3\phi_2}{a_1^2a_2\partial\xi^{2}{}_{1}\partial\xi_2}\right)-\frac{B_{11}}{R_2}\frac{\partial u}{a_1\,\partial\xi_1}-\frac{B_{12}}{R_1}\frac{\partial v}{a_2\partial\xi_2}+B_{16}\frac{\partial^3 u}{a_2^2a_1\partial\xi_2^{\,2}\partial\xi_1}+B_{18}\frac{\partial^3 v}{a_1^2a_2\partial\xi^{2}{}_{1}\partial\xi_2}+\\
&-\frac{C_4}{R^{2}{}_{2}}w-\frac{C_5}{R_2}\left(y^*\frac{\partial\phi_2}{a_2\partial\xi_2}-\frac{2\partial^2 w}{a_2^2\partial\xi_2^{\,2}}\right)+C_6\left(y^*\frac{\partial^3\phi_2}{a_2^3\partial\xi^{3}{}_{2}}-\frac{\partial^4 w}{a_2^4\partial\xi_2^{\,4}}\right)-\frac{C_8}{R_2}\frac{\partial\phi_2}{a_2\partial\xi_2}+C_9\frac{\partial^3\phi_2}{a_2^3\partial\xi^{3}{}_{2}}-\frac{C_{12}}{R_2}\frac{\partial v}{a_2\partial\xi_2}+C_{18}\frac{\partial^3 v}{a_2^3\partial\xi^{3}{}_{2}}+\\
&+2D_6\left(y^*\left(\frac{\partial^3\phi_1}{a_1\,a_2^2\partial\xi_1\partial\xi^{2}{}_{2}}+\frac{\partial^3\phi_2}{a_1^2a_2\partial\xi^{2}{}_{1}\partial\xi_2}\right)-\frac{2\partial^4 w}{a_1^2a_2^2\partial\xi_1^{\,2}\partial\xi^{2}{}_{2}}\right)+\\
&+2D_9\left(\frac{\partial^3\phi_1}{a_1\,a_2^2\partial\xi^{2}{}_{2}\partial\xi_1}+\frac{\partial^3\phi_2}{a_1^2a_2\partial\xi^{2}{}_{1}\partial\xi_2}\right)+2D_{16}\frac{\partial^3 u}{a_1\,a_2^2\partial\xi_1\partial\xi^{2}{}_{2}}+2D_{18}\frac{\partial^3 v}{a_1^2a_2\partial\xi^{2}{}_{1}\partial\xi_2}=\left(1-\mu^2\nabla^2\right)(-q)
\end{aligned}
\tag{15c}
$$

$$
\begin{aligned}
&\frac{A_5y^*}{R_1}\frac{\partial w}{a_1\,\partial\xi_1}+A_6y^*\left(y^*\frac{\partial^2\phi_1}{a_1^2\partial\xi^{2}{}_{1}}-\frac{\partial^3 w}{a_1^3\partial\xi_1^{\,3}}\right)+\frac{A_8}{R_1}\frac{\partial w}{a_1\,\partial\xi_1}+A_9\left(2y^*\frac{\partial^2\phi_1}{a_1^2\partial\xi^{2}{}_{1}}-\frac{\partial^3 w}{a_1^3\partial\xi_1^{\,3}}\right)+A_{10}\frac{\partial^2\phi_1}{a_1^2\partial\xi^{2}{}_{1}}+\\
&+A_{16}y^*\frac{\partial^2 u}{a_1^2\partial\xi^{2}{}_{1}}+A_{17}\frac{\partial^2 u}{a_1^2\partial\xi^{2}{}_{1}}+\frac{B_5y^*}{R_2}\frac{\partial w}{a_1\,\partial\xi_1}+B_6y^*\left(y^*\frac{\partial^2\phi_2}{a_1\,a_2\partial\xi_1\partial\xi_2}-\frac{\partial^3 w}{a_1\,a_2^2\partial\xi_1\partial\xi_2^{\,2}}\right)+\frac{B_8}{R_2}\frac{\partial w}{a_1\,\partial\xi_1}+\\
&+B_9\left(2y^*\frac{\partial^2\phi_2}{a_1\,a_2\partial\xi_1\partial\xi_2}-\frac{\partial^3 w}{a_1\,a_2^2\partial\xi_1\partial\xi_2^{\,2}}\right)+B_{10}\frac{\partial^2\phi_2}{a_1\,a_2\partial\xi_1\partial\xi_2}+B_{18}y^*\frac{\partial^2 v}{a_1\,a_2\partial\xi_1\partial\xi_2}+B_{19}\frac{\partial^2 v}{a_1\,a_2\partial\xi_1\partial\xi_2}+\\
&+D_6y^*\left(y^*\left(\frac{\partial^2\phi_1}{a_2^2\partial\xi^{2}{}_{2}}+\frac{\partial^2\phi_2}{a_1\,a_2\partial\xi_1\partial\xi_2}\right)-\frac{2\partial^3 w}{a_1\,a_2^2\partial\xi_1\partial\xi^{2}{}_{2}}\right)+2D_9\left(y^*\left(\frac{\partial^2\phi_1}{a_2^2\partial\xi^{2}{}_{2}}+\frac{\partial^2\phi_2}{a_1\,a_2\partial\xi_1\partial\xi_2}\right)-\frac{\partial^3 w}{a_1\,a_2^2\partial\xi_1\partial\xi^{2}{}_{2}}\right)+\\
&+D_{10}\left(\frac{\partial^2\phi_1}{a_2^2\partial\xi^{2}{}_{2}}+\frac{\partial^2\phi_2}{a_1\,a_2\partial\xi_1\partial\xi_2}\right)+D_{16}y^*\frac{\partial^2 u}{a_2^2\partial\xi^{2}{}_{2}}+D_{17}\frac{\partial^2 u}{a_2^2\partial\xi^{2}{}_{2}}+D_{18}y^*\frac{\partial^2 v}{a_1\,a_2\partial\xi_1\partial\xi_2}+D_{19}\frac{\partial^2 v}{a_1\,a_2\partial\xi_1\partial\xi_2}+\\
&-G_{11}y^*\left(\frac{1}{R_1}u+y^*\phi_1\right)-G_{13}\left(\frac{1}{R_1}u+2y^*\phi_1\right)-G_{14}\phi_1=0
\end{aligned}
\tag{15d}
$$

$$\begin{aligned}
&\frac{B_5 y^*}{R_1}\frac{\partial w}{a_2\partial\xi_2}+B_6 y^*\left(y^*\frac{\partial^2\phi_1}{a_1 a_2\partial\xi_1\partial\xi_2}-\frac{\partial^3 w}{a_1^2 a_2\partial\xi_1{}^2\partial\xi_2}\right)+\frac{B_8}{R_1}\frac{\partial w}{a_2\partial\xi_2}+B_9\left(2y^*\frac{\partial^2\phi_1}{a_1 a_2\partial\xi_1\partial\xi_2}-\frac{\partial^3 w}{a_1^2 a_2\partial\xi_1{}^2\partial\xi_2}\right)+\\
&+B_{10}\frac{\partial^2\phi_1}{a_1 a_2\partial\xi_1\partial\xi_2}+B_{16}y^*\frac{\partial^2 u}{a_1 a_2\partial\xi_1\partial\xi_2}+B_{17}\frac{\partial^2 u}{a_1 a_2\partial\xi_1\partial\xi_2}+\frac{C_5 y^*}{R_2}\frac{\partial w}{a_2\partial\xi_2}+C_6 y^*\left(y^*\frac{\partial^2\phi_2}{a_2^2\partial\xi^2{}_2}-\frac{\partial^3 w}{a_2^3\partial\xi_2{}^3}\right)+\\
&+\frac{C_8}{R_2}\frac{\partial w}{a_2\partial\xi_2}+C_9\left(2y^*\frac{\partial^2\phi_2}{a_2^2\partial\xi^2{}_2}-\frac{\partial^3 w}{a_2^3\partial\xi_2{}^3}\right)+C_{10}\frac{\partial^2\phi_2}{a_2^2\partial\xi^2{}_2}+C_{18}y^*\frac{\partial^2 v}{a_2^2\partial\xi^2{}_2}+C_{19}\frac{\partial^2 v}{a_2^2\partial\xi^2{}_2}+\\
&+D_6 y^*\left(y^*\left(\frac{\partial^2\phi_1}{a_1 a_2\partial\xi_1\partial\xi_2}+\frac{\partial^2\phi_2}{a_1^2\partial\xi^2{}_1}\right)-\frac{2\partial^3 w}{a_1^2 a_2\partial\xi^2{}_1\partial\xi_2}\right)+2D_9\left(y^*\left(\frac{\partial^2\phi_1}{a_1 a_2\partial\xi_1\partial\xi_2}+\frac{\partial^2\phi_2}{a_1^2\partial\xi^2{}_1}\right)-\frac{\partial^3 w}{a_1^2 a_2\partial\xi^2{}_1\partial\xi_2}\right)+\\
&+D_{10}\left(\frac{\partial^2\phi_1}{a_1 a_2\partial\xi_1\partial\xi_2}+\frac{\partial^2\phi_2}{a_1^2\partial\xi^2{}_1}\right)+D_{16}y^*\frac{\partial^2 u}{a_1 a_2\partial\xi_2\partial\xi_1}+D_{17}\frac{\partial^2 u}{a_1 a_2\partial\xi_2\partial\xi_1}+D_{18}y^*\frac{\partial^2 v}{a_1^2\partial\xi^2{}_1}+\\
&+D_{19}\frac{\partial^2 v}{a_1^2\partial\xi^2{}_1}-F_{11}y^*\left(\frac{1}{R_2}v+y^*\phi_2\right)-F_{13}\left(\frac{1}{R_2}v+2y^*\phi_2\right)-F_{14}\phi_2=0
\end{aligned} \tag{15e}$$

More details about the parameters of Equation 15(a)–(e) are provided in Appendix A. The mathematical background defined in this case has been implemented and solved numerically by using a Navier type procedure, as specified in the following.

3. Solution Procedure

Since the exact solution of the partial differential Equation 15(a)–(e) determined in Section 2, for general boundary conditions is difficult, a Navier-type solution is applied for simply-supported doubly-curved nanoshells in this scenario. Thus, the equations related to boundary conditions are defined by the equation below.

$$\begin{aligned}
&u(\xi_1,0)=u(\xi_1,b)=v(0,\xi_2)=v(a,\xi_2)=0\\
&w(\xi_1,0)=w(\xi_1,b)=w(0,\xi_2)=w(a,\xi_2)=0\\
&\phi_1(\xi_1,0)=\phi_1(\xi_1,b)=\phi_2(0,\xi_2)=\phi_2(a,\xi_2)=0
\end{aligned} \tag{16}$$

Based on Equation (16), the solution functions to the partial differential Equation 15(a)–(e) can be expressed by the equation below [54,55].

$$\begin{aligned}
u(\xi_1,\xi_2;t)&=\sum_{r=1}^{\infty}\sum_{s=1}^{\infty} U_{rs}\cos(\alpha\xi_1)\sin(\beta\xi_2)\\
v(\xi_1,\xi_2;t)&=\sum_{r=1}^{\infty}\sum_{s=1}^{\infty} V_{rs}\sin(\alpha\xi_1)\cos(\beta\xi_2)\\
w(\xi_1,\xi_2;t)&=\sum_{r=1}^{\infty}\sum_{s=1}^{\infty} W_{rs}\sin(\alpha\xi_1)\sin(\beta\xi_2)\\
\phi_1(\xi_1,\xi_2;t)&=\sum_{r=1}^{\infty}\sum_{s=1}^{\infty} \phi_{rs}^1\cos(\alpha\xi_1)\sin(\beta\xi_2)\\
\phi_2(\xi_1,\xi_2;t)&=\sum_{r=1}^{\infty}\sum_{s=1}^{\infty} \phi_{rs}^2\sin(\alpha\xi_1)\cos(\beta\xi_2)
\end{aligned} \tag{17}$$

where

$$\alpha=\frac{r\pi}{a},\ \beta=\frac{s\pi}{b} \tag{18}$$

Substituting Equation (17) into Equation 15(a)–(e), the following equations are derived.

$$\left[K_{ij}\right]\begin{Bmatrix} U_{rs} \\ V_{rs} \\ W_{rs} \\ \phi_{rs}^{1} \\ \phi_{rs}^{2} \end{Bmatrix} = \begin{Bmatrix} 0 \\ 0 \\ Q_{rs} \\ 0 \\ 0 \end{Bmatrix}, \quad (i, j = 1,2,..,5) \tag{19}$$

where U_{rs}, V_{rs}, W_{rs}, ϕ_{rs}^{1}, and ϕ_{rs}^{2} are the unknown coefficients. $\left[K_{ij}\right]$ is the stiffness matrix, whose additional details are provided in Appendix B. Q_{rs} are the coefficients in the double Fourier expansion related to the transverse load, i.e.,

$$q(x,y) = \sum_{r=1}^{\infty}\sum_{s=1}^{\infty} Q_{rs}\sin(\alpha x_1)\sin(\beta x_2) \tag{20}$$

4. Numerical Results and Discussion

This section is devoted, first, to validate the proposed theory, and then, to evaluate the sensitivity of the static response of symmetric doubly-curved nanoshells by means of a systematic study. The results obtained in the following are divided in two categories, namely, shallow and deep nanoshells. The governing equations of the problem, defined by Equation (19), in compact form, together with its stiffness matrix detailed in Appendix B, are implemented and solved in a MATLAB subroutine in this scenario. The effect of several parameters, such as the nonlocal parameter, the mechanical and geometrical properties, is, thus, investigated on the bending deflection of isotropic doubly-curved shallow and deep nanoshells, while comparing their final response.

4.1. Comparison and Validation

This section is devoted to the validation and parametric study of the static behavior of doubly-curved nanoshells. For validation purposes, we determine the deflection and stress response in dimensionless form in agreement with References [56–60], as follows.

$$\begin{aligned} \bar{w} &= w\left(\frac{a}{2},\frac{b}{2},0\right)\frac{10^2 E h^3}{q_0 a^4}, \quad \bar{\sigma}_{xx} = \sigma_{xx}\left(\frac{a}{2},\frac{b}{2},\frac{h}{2}\right)\frac{h^2}{q_0 a^2} \\ \bar{\tau}_{xy} &= \tau_{xy}\left(0,0,\frac{h}{2}\right)\frac{h^2}{q_0 a^2}, \quad \bar{\tau}_{xz} = \tau_{xz}\left(0,\frac{b}{2},0\right)\frac{h}{q_0 a}, \quad \bar{z} = \frac{z}{h}\times 10 \end{aligned} \tag{21}$$

The deflection response is evaluated comparatively between a nonlocal and local theory. Table 1 summarizes the deflection and stress results for square plates under a uniform load, and different side-to-thickness ratios a/h. This example represents the limit case for a doubly-curved nanoshell, when the curvature radii tends to infinite values ($R_1 = R_2 \to \infty$). The numerical results based on our proposed formulation are in line with predictions by Reddy [56,57], Ferreira et al. [58,59], and Xiang et al. [60], where the proposed HSDT yield results in terms of deflection and a stress response. As notable in Table 1, an increased a/h ratio enables a general decrease in the non-dimensional deflection of the plate, and an overall increase in the stress value, which is in agreement with findings by References [56–60]. A similar parametric study is repeated for symmetric doubly-curved shells under a sinusoidal lateral loading, as summarized in Table 2. The results are successfully verified against predictions based on a parabolic shear deformation theory (PSDT) and classical thin shell theory (CST), as shown in Reference [61]. Based on results in Table 2, it is visible that an increased R/a ratio enables a general increase in the non-dimensional deflection of the doubly-curved shell, for each fixed value for h/a ratio, whereby, an increased h/a ratio decreases the overall structural deflection due to the increased stiffness of the curved shells. The accuracy of our proposed theory against the available literature [61] is confirmed once again by good agreement between results in Table 2.

Table 1. Non-dimensional deflection and stress state for square isotropic plates under a uniform load.

$\frac{a}{h}$	**Method**	$\bar{w}$	$\bar{\sigma}_{xx}$
10	Exact [56]	4.791	0.2762
	Reddy [57]	4.77	0.2899
	Ferreira et al. [58]	4.787	0.2739
	Ferreira et al. [59]	4.788	0.2762
	Xiang et al. [60]	4.609	0.288
	present	4.758	0.3193
20	Exact [56]	4.625	0.2762
	Reddy [57]	4.57	0.2683
	Ferreira et al. [58]	4.613	0.2737
	Ferreira et al. [59]	4.616	0.2749
	Xiang et al. [60]	4.442	0.276
	present	4.587	0.32
50	Exact [56]	4.579	0.2762
	Reddy [57]	4.496	0.2667
	Ferreira et al. [58]	4.575	0.2787
	Ferreira et al. [59]	4.578	0.2745
	Xiang et al. [60]	4.396	0.284
	present	4.55	0.3203
100	Exact [56]	4.572	0.2762
	Reddy [57]	4.482	0.2664
	Ferreira et al. [58]	4.573	0.2844
	Ferreira et al. [59]	4.5715	0.2744
	Xiang et al. [60]	-	0.282
	present	4.5455	0.3203

Table 2. Non-dimensional deflection of doubly-curved shallow shells under a sinusoidal distribution of the lateral loading.

R / a	**Method**	$h / a = 0.01$	$h / a = 0.1$	$h / a = 0.15$
1	Present	98.1142	7.4312	3.877
	3-D [61]	100.59	8.7095	4.9497
	PSDT [61]	99.645	7.4751	3.8929
	CST [61]	99.644	7.3702	3.6979
2	Present	392.8533	16.9774	6.8716
	3-D [61]	396.45	18.451	7.724
	PSDT [61]	394.37	17.013	6.9261
	CST [61]	394.37	16.48	6.3322
3	Present	870.5856	22.1878	8.0018
	3-D [61]	875.36	23.381	8.5912
	PSDT [61]	872.02	22.277	8.094
	CST [61]	872	21.371	7.2945
4	Present	1512.3	24.8495	8.4892
	3-D [61]	1518.3	25.785	8.9235
	PSDT [61]	1513.6	24.983	8.6017
	CST [61]	1513.6	23.849	7.7043
5	Present	2294.2	26.3088	8.7352
	3-D [61]	2301.4	27.061	9.0755
	PSDT [61]	2295.4	26.471	8.8589
	CST [61]	2295.3	25.201	7.9099
10	Present	7370.9	28.5417	9.0861
	3-D [61]	7383.1	28.91	9.2502
	PSDT [61]	7371.3	28.754	9.2267
	CST [61]	7370.2	27.262	8.2019
20	Present	16,485	29.1602	9.1782
	3-D [61]	16,499	29.356	9.2666
	PSDT [61]	16,485	29.388	9.3235
	CST [61]	16,479	27.831	8.2783
∞	Present	28,039	29.3723	9.2094
	3-D [61]	29,504	29.44	9.2352
	PSDT [61]	28,041	29.606	9.3562
	CST [61]	28,026	28.026	8.304

4.2. Static Analysis of Doubly-Curved thin Nanoshells

This subsection studies the mechanical behavior of doubly-curved thin nanoshells, and its sensitivity to the nonlocal and geometrical properties of the nanostructures.

In Figure 2a–c, we present the evolution of the stress components in a non-dimensional form, throughout the thickness for a thin spherical panel with different nonlocal parameters. Based on these figures, it is worth observing that the stiffness decreases for an increasing nonlocal parameter, along with a general decrease in the natural frequency of the nanostructure, and an increase in the stress components. More specifically, the nonlocal parameter affects the axial and longitudinal shear stress more significantly near the top and bottom sides of the panel, while assuming a null value at the mid-plane, independently of the nonlocal parameter (Figure 2a,b). The contrary occurs for the shear stress component, whose value remains unaltered and equal to zero at both extremity sides, and reaches the peak value at the mid-plane with an increasing magnitude for an increased nonlocal parameter (Figure 2c).

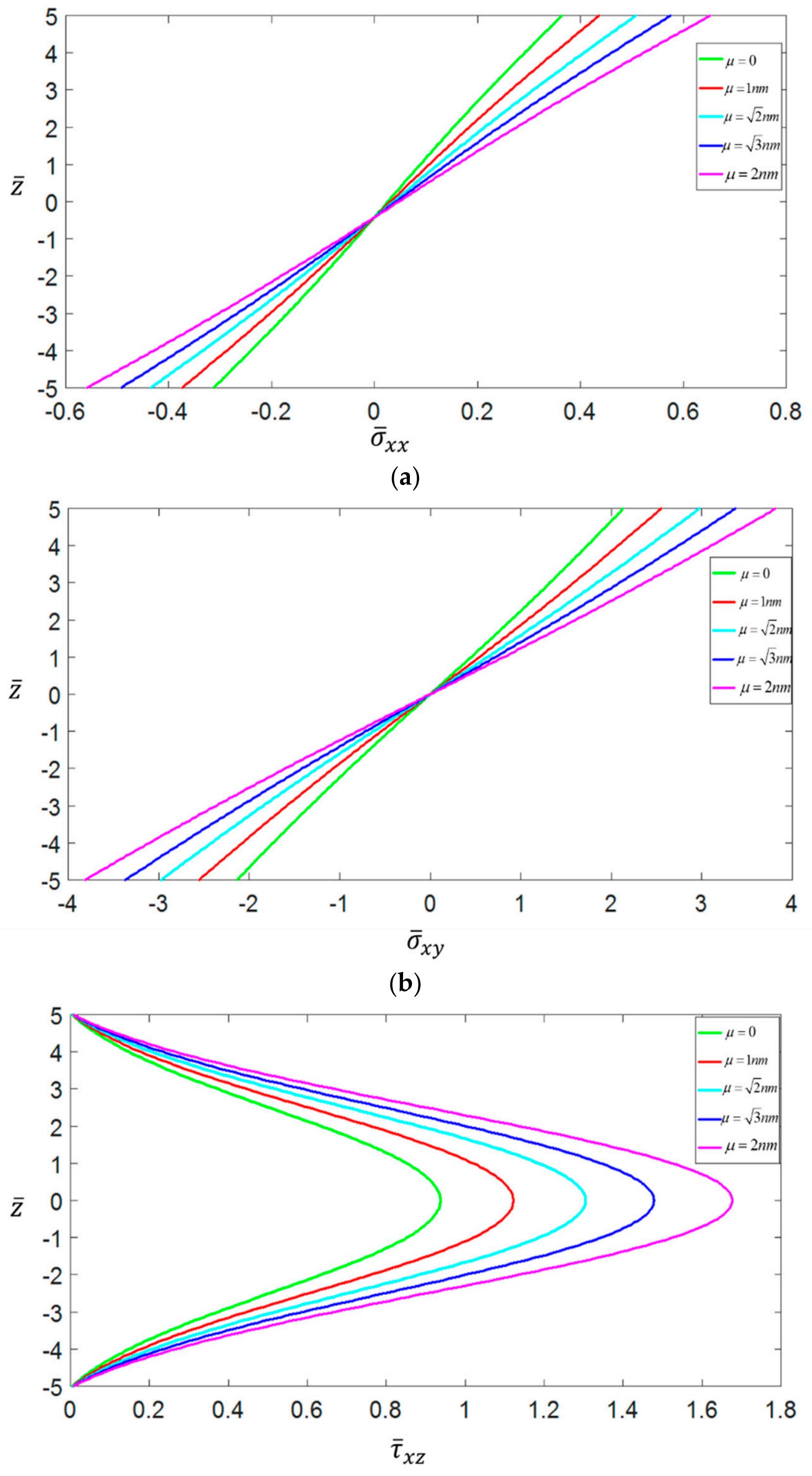

Figure 2. Variation with the nonlocal parameter of the dimensionless axial stress (**a**), longitudinal shear stress (**b**), and transverse shear stress (**c**) through the thickness of shallow spherical panels with $R_1 = R_2, R/a = 10, a/h = 10$.

Figure 3 also shows the combined effect of the nonlocal parameter, μ, and side-to-thickness ratio, a/h, on the deflection response of thin spherical (Figure 3a) and cylindrical (Figure 3b) panels. In both cases, an increased non-local parameter clearly yields a monotonic increase in deflection for each fixed a/h ratio. The deflection also increases for a decreased geometrical a/h ratio, while keeping the nonlocal parameter fixed due to an overall stiffness reduction. Based on a comparative evaluation of the curves in Figure 3a,b under the same assumptions for μ and a/h, the spherical panels seem to be more flexible than the cylindrical panels due to the higher deflections registered for the first geometry. This is in line with the well-known size-dependence of the mechanical properties for small-scaled structures and nanoelectromechanical systems (NEMS), as largely observed in many experimental investigations and atomistic simulations in literature.

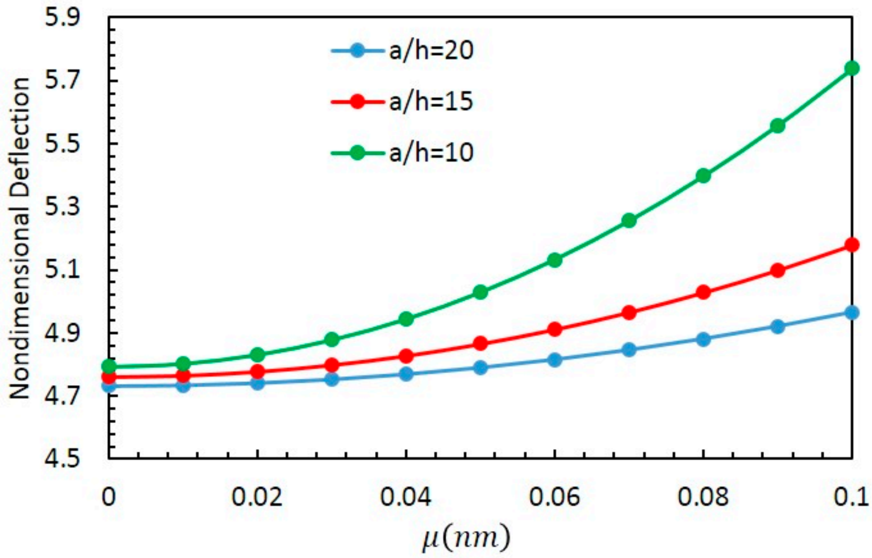

(**a**)

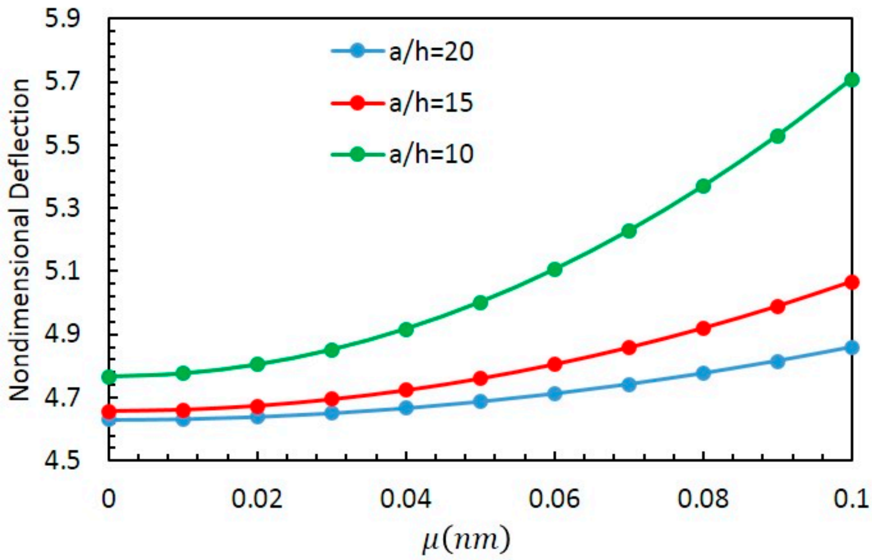

(**b**)

Figure 3. Effect of the nonlocal parameter and a/h ratio on the deflection of shallow (**a**) spherical panels with $R_1 = R_2, R/a = 20$, and (**b**) cylindrical panels with $R_1/a = 20, R_2 \to \infty$.

In Figure 4a,b, we plot the effect of the nonlocal parameter and Poisson's ratio on the deflection of the shallow spherical panel and cylindrical panel, respectively, under a uniform load. Both figures clearly show that the structural deflection increases with the nonlocal parameter under a fixed Poisson's ratio, whereby an increased value of the Poisson's ratio reduces the structural deformability under a fixed nonlocal parameter. The double effect of the nonlocal parameter and length-to-side ratio b/a is also considered in Figure 5a,b, for a shallow spherical or cylindrical panel, respectively, whose deflection seems to increase for an increased nonlocal parameter and length-to-side ratio. By comparing Figure 5a,b, it is worth noticing the higher deformability of spherical panels compared to cylindrical panels under the same assumptions of the μ and b/a ratio. This variation in stiffness is simply related to topological reasons, which is more pronounced for increasing the ratios b/a, as visible in the plots of Figure 5a,b.

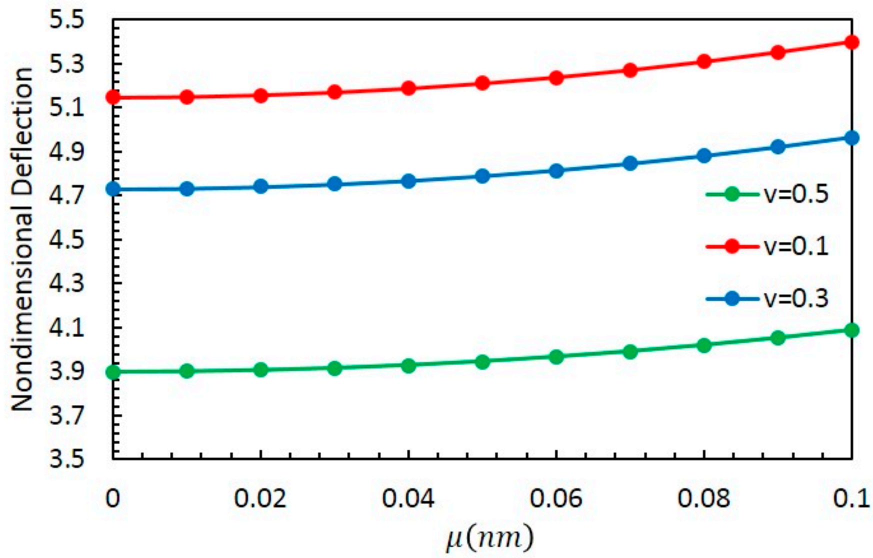

(**a**)

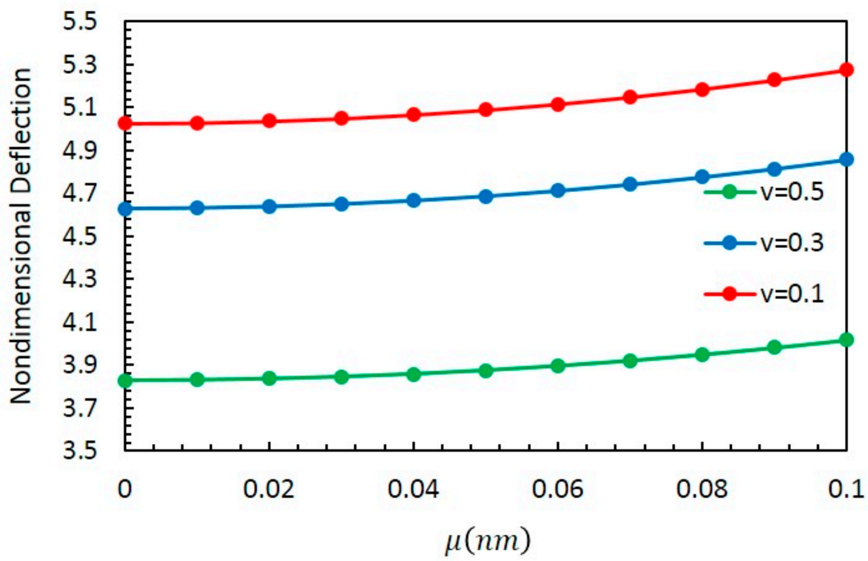

(**b**)

Figure 4. Effect of the nonlocal parameter and Poisson's coefficient on the deflection of shallow (**a**) spherical panels with $R_1 = R_2, R/a = 20, a/h = 20$, (**b**) cylindrical panels with $R_1/a = 20, R_2 \to \infty, a/h = 20$.

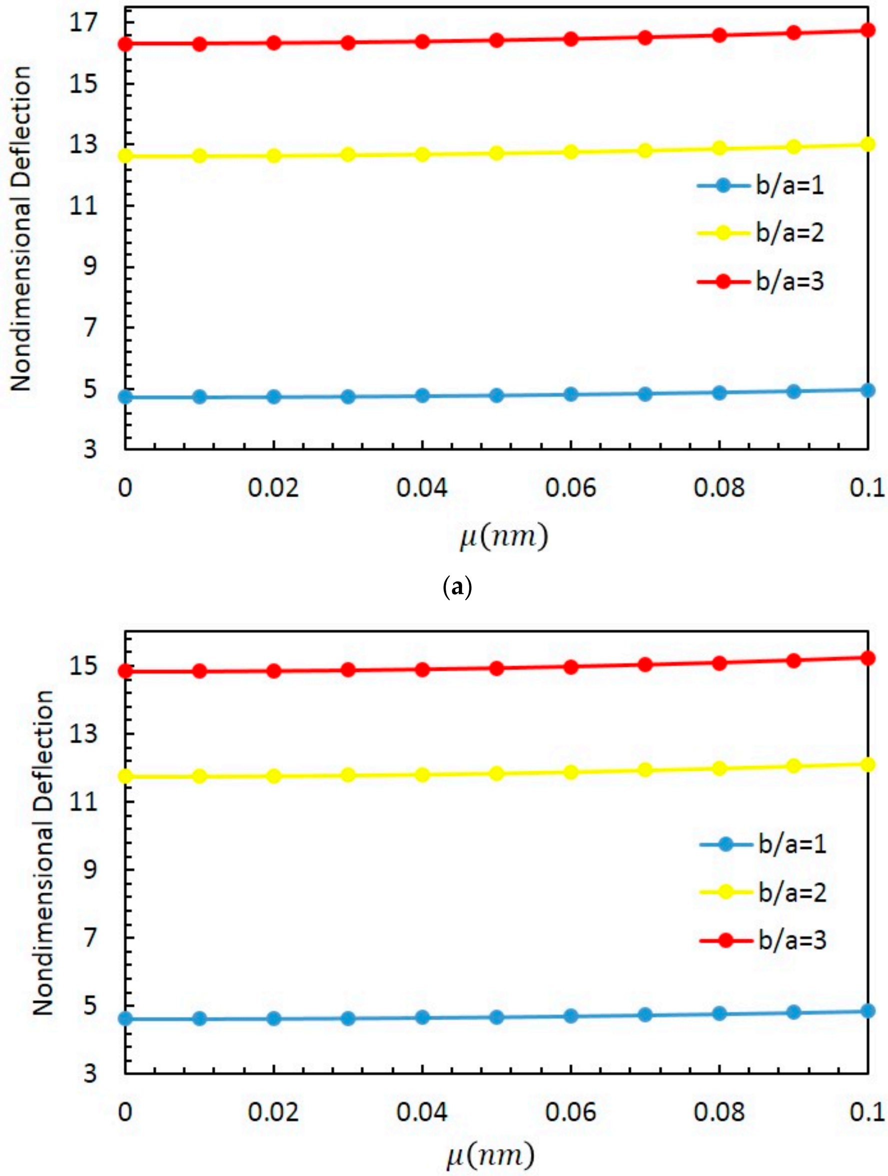

(**a**)

(**b**)

Figure 5. Effect of the nonlocal parameter and b/a ratio on the deflection of shallow (**a**) spherical panels with $R_1 = R_2, R/a = 20$, and (**b**) cylindrical panels with $R_1/a = 20, R_2 \to \infty$.

Tables 3 and 4 summarize the results in terms of a deflection response for a thin ($a/h = 20$) and moderately thick ($a/h = 10$) shallow spherical (Table 3) and cylindrical (Table 4) panel, under a uniform load, with different nonlocal parameters, side-to-thickness ratios (R/a), and length-to-side ratios (b/a). As visible in both tables, the deflection response of shallow panels increases for an increased nonlocal parameter as well as for a decreased R/a ratio and an increased b/a ratio due to a global decreased structural stiffness. From a physical standpoint, these results would confirm the importance of a correct definition of nonlocality parameters within nanostructures by means of appropriate experimental tests for different geometries, which could considerably affect the global structural stiffness and functionality of nanosystems.

Table 3. Non-dimensional deflection of shallow spherical panels ($\tilde{w} = w\left(10^2 Eh^3\right)/\left(q_0 a^4\right)$) under a uniform load.

μ	R/a	$b/a=1$		$b/a=2$		$b/a=3$	
		$a/h=10$	$a/h=20$	$a/h=10$	$a/h=20$	$a/h=10$	$a/h=20$
0.25	5	12.0386	11.0094	30.0962	28.7524	40.5842	38.0363
	10	10.9468	6.7840	22.8961	19.6583	28.0741	27.3571
	20	10.7041	6.1901	21.6039	15.0639	26.0654	19.1014
	50	10.6381	6.0420	21.2679	14.1387	25.5534	17.6132
	100	10.6287	6.0214	21.2207	14.0157	25.4819	17.4193
	plate	10.6256	6.0146	21.2050	13.9752	25.4582	17.3556
0.5	5	31.9859	18.7949	69.4048	42.6926	90.0968	54.7284
	10	29.0851	11.5815	52.8006	29.1893	62.3243	39.3627
	20	28.4402	10.5675	49.8209	22.3674	57.8650	27.4840
	50	28.2648	10.3147	49.0459	20.9936	56.7285	25.3427
	100	28.2399	10.2796	48.9371	20.811	56.5698	25.0637
	plate	28.2316	10.2679	48.9010	20.7508	56.5171	24.9721
0.75	5	65.2313	31.7707	134.9192	65.9262	172.6177	82.5485
	10	59.3154	19.5772	102.6416	45.0744	119.4080	59.3719
	20	58.0004	17.8633	96.8491	34.540	110.8644	41.4551
	50	57.6426	17.4359	95.3426	32.4185	108.6870	38.2252
	100	57.5918	17.3765	95.1312	32.1365	108.3829	37.8044
	plate	57.5749	17.3567	95.0609	32.0436	108.2819	37.6662
1	5	111.7749	49.9368	226.6394	98.4534	288.1471	121.4968
	10	101.6379	30.7713	172.4189	67.3136	199.3252	87.3849
	20	99.3836	28.0773	162.6887	51.5815	185.0636	61.0145
	50	98.7715	27.4055	160.1579	48.4134	181.4289	56.2606
	100	98.6845	27.3121	159.8028	47.9923	180.9213	55.6413
	plate	98.6555	27.2811	159.6848	47.8535	180.7527	55.4379

Table 4. Non-dimensional deflection of shallow cylindrical panels ($\tilde{w} = w\left(10^2 Eh^3\right)/\left(q_0 a^4\right)$) under a uniform load.

μ	R_1/a	$b/a=1$		$b/a=2$		$b/a=3$	
		$a/h=10$	$a/h=20$	$a/h=10$	$a/h=20$	$a/h=10$	$a/h=20$
0.25	5	10.9468	6.784	21.4586	14.6529	25.5534	17.6132
	10	10.7041	6.1901	21.2679	14.1387	25.4819	17.4193
	20	10.6451	6.0575	21.2207	14.0157	25.4641	17.3715
	50	10.6287	6.0214	21.2076	13.9816	25.4592	17.3582
	100	10.6264	6.0163	21.2057	13.9768	25.4584	17.3563
	plate	10.6256	6.0146	21.205	13.9752	25.4582	17.3556
0.5	5	29.0851	11.5815	49.4858	21.7572	56.7285	25.3427
	10	28.4402	10.5675	49.0459	20.9936	56.5698	25.0637
	20	28.2835	10.3412	48.9371	20.811	56.5303	24.9949
	50	28.2399	10.2796	48.9068	20.7604	56.5192	24.9757
	100	28.2337	10.2708	48.9024	20.7532	56.5176	24.973
	plate	28.2316	10.2679	48.901	20.7508	56.5171	24.9721
0.75	5	59.3154	19.5772	96.1977	33.5977	108.687	38.2252
	10	58.0004	17.8633	95.3426	32.4185	108.3829	37.8044
	20	57.6807	17.4807	95.1312	32.1365	108.3072	37.7006
	50	57.5918	17.3765	95.0721	32.0584	108.286	37.6717
	100	57.5791	17.3617	95.0637	32.0473	108.2829	37.6675
	plate	57.5749	17.3567	95.0609	32.0436	108.2819	37.6662
1	5	101.6379	30.7713	161.5943	50.1744	181.4289	56.2606
	10	99.3846	28.0773	160.1579	48.4134	180.9213	55.6413
	20	98.8368	27.4759	159.8028	47.9923	180.7948	55.4886
	50	98.6845	27.3121	159.7037	47.8757	180.7594	55.446
	100	98.6628	27.2889	159.6895	47.8591	180.7544	55.4399
	plate	98.6555	27.2811	159.6848	47.8535	180.7527	55.4379

The systematic study of the deflection response for shallow spherical and cylindrical panels under a uniform loading condition is finally plotted in Figure 6a,b, respectively, for different nonlocal parameters and side-to-thickness ratios a/h. Based on the histograms of Figure 6, the deflection response seems to be almost unaffected by the a/h ratio, under a fixed nonlocal parameter μ, while being significantly affected by the nonlocal parameter with a gradual increase in flexibility for increasing values of μ under the same assumption for a/h.

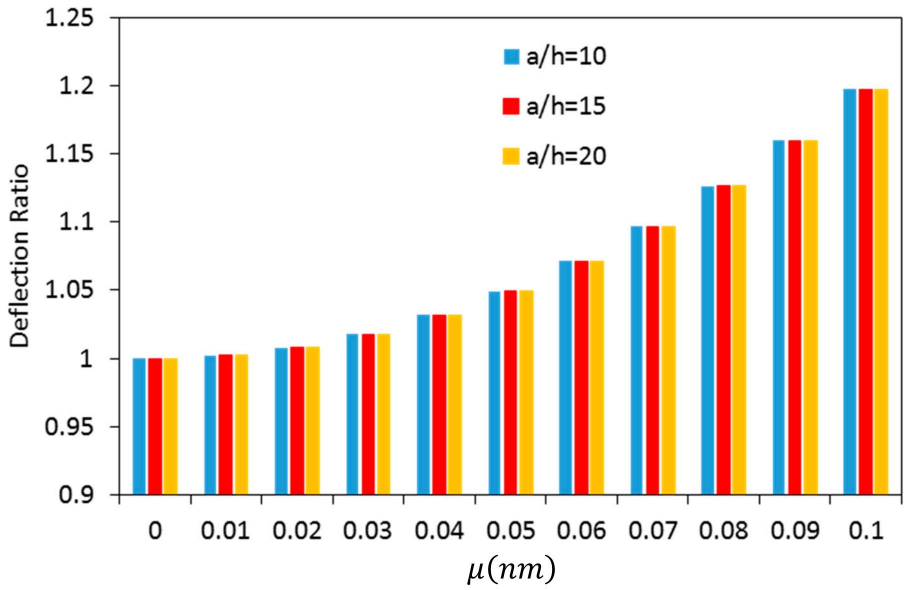

(**a**)

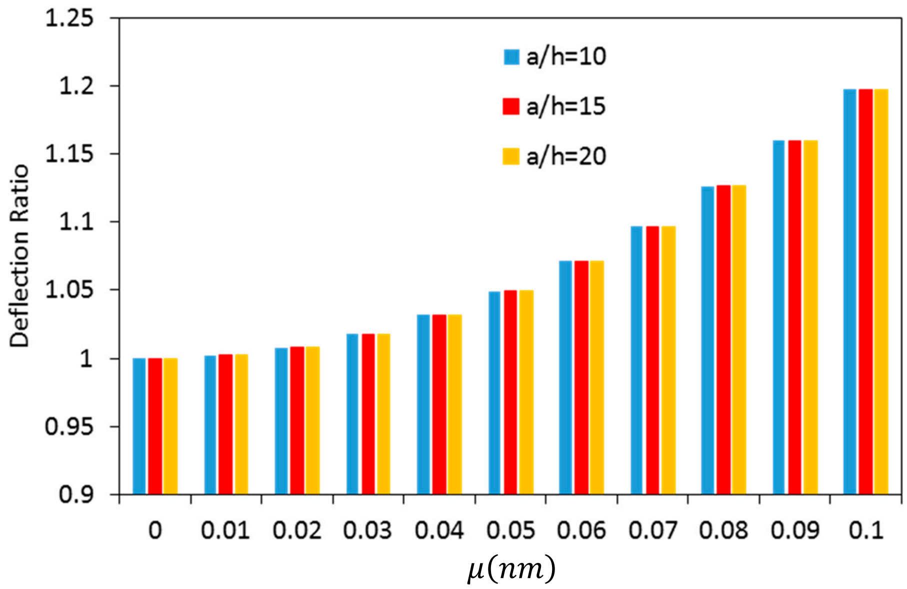

(**b**)

Figure 6. Effect of the nonlocal parameter and a/h ratio on the deflection ratio of shallow (**a**) spherical panels with $R_1 = R_2, R/a = 20$, and (**b**) cylindrical panels with $R_1/a = 20, R_2 \to \infty$.

4.3. Static Analysis of Doubly-Curved Deep Nanoshells

The same unified formulation is applied in this subsection to study the structural response of doubly-curved deep nanoshells with $R / a \leq 5$. In Figure 7a–c, we plot the distribution of the non-dimensional stress components throughout the thickness for a deep spherical panel and for a varying nonlocal parameter. According to results in Figure 7a–c, an increased nonlocal parameter clearly yields a decreased structural stiffness, a decreased natural frequency, and an overall increase in the axial (Figure 7a), longitudinal, and transverse shear (Figure 7b,c) stress components. More specifically, the transverse shear stress assumes its highest value at the mid-plane, whereby the axial and longitudinal shear stresses are reached at the top and bottom sides, while featuring higher values for a shallow spherical panel compared to the deep one. Once again, this variation in stress distribution for different nonlocalities can clearly affect the global stiffness of a nanostructure, and must be carefully accounted for design purposes.

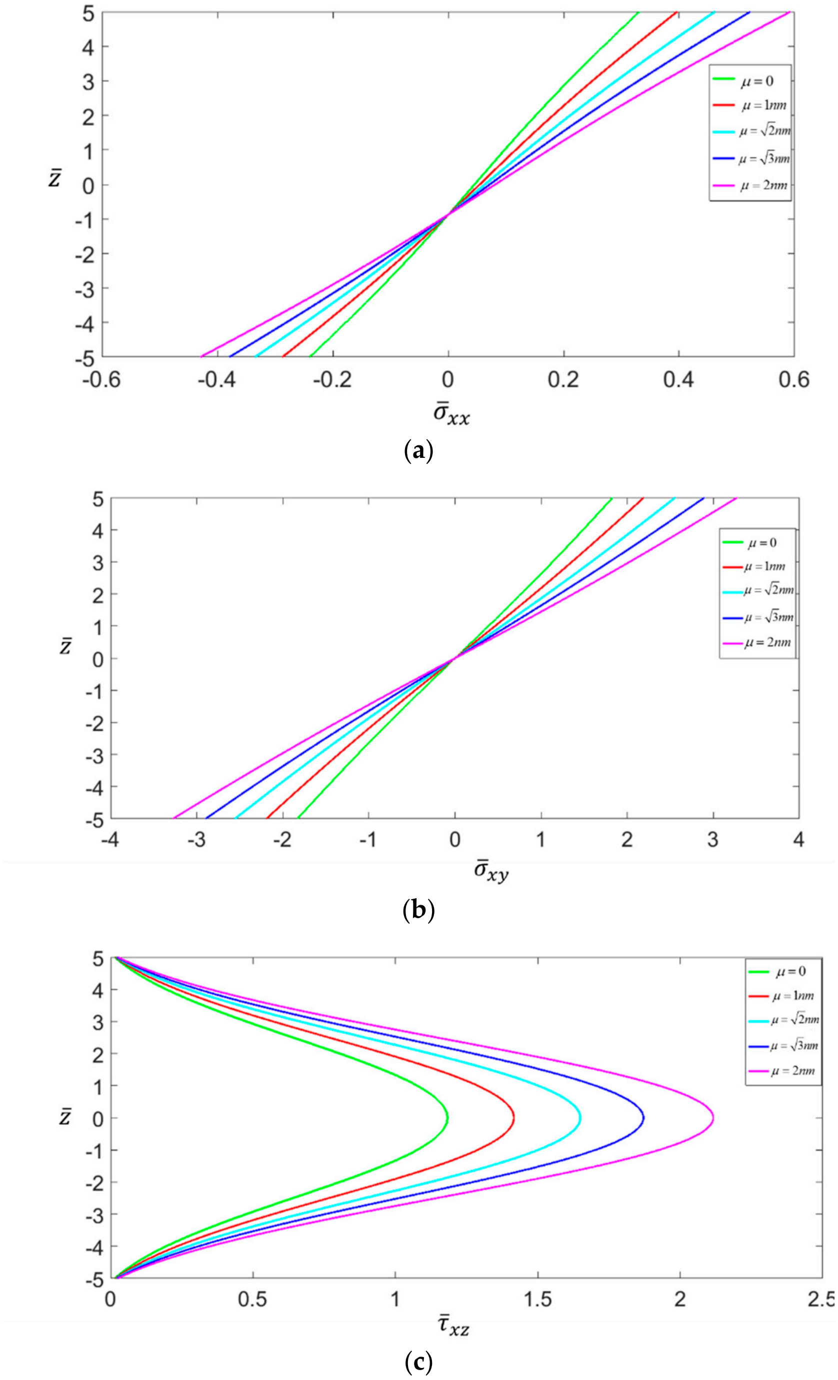

Figure 7. Variation with the nonlocal parameter of the dimensionless axial stress (**a**), longitudinal shear stress (**b**), and transverse shear stress (**c**), through the thickness of deep spherical panels with $R_1 = R_2, R/a = 5, a/h = 10$.

Table 5 summarizes the effect of the nonlocal parameter, and length-to-width ratio b/a on the deflection of a thick ($a/h = 5$) and moderately thick ($a/h = 10$) deep spherical panel under a uniform load. Based on the results in Table 5, the non-dimensional deflection clearly increases with the nonlocal parameter due to the reduced structural stiffness. In addition, the deformability of the deep spherical panel seems to reduce for an increased a/h ratio and a decreased b/a ratio. Based on a comparative evaluation of Tables 3 and 5, it can be concluded that the deflection of shallow panels is greater than deep panels, or equivalently shallow panels are more flexible than deep counterparts. As plotted in Figure 8, the non-dimensional deflection of the deep spherical panel increases for an increased nonlocal parameter, and length-to-side ratio.

Table 5. Non-dimensional deflection of deep spherical panels ($\tilde{w} = w\left(10^2 Eh^3\right)/\left(q_0 a^4\right)$) under a uniform load. $R_1 = R_2, R/a = 5$.

$\mu(nm)$	$b/a=1$		$b/a=2$		$b/a=3$	
	$a/h=5$	$a/h=10$	$a/h=5$	$a/h=10$	$a/h=5$	$a/h=10$
0	5.2322	4.2624	12.0728	9.2637	14.8348	11.0326
0.1	6.265	5.1038	13.5622	10.4066	16.4617	12.2425
0.2	9.3633	7.6279	18.0305	13.8352	21.3421	15.872
0.3	14.5273	11.8347	25.4776	19.5495	29.4762	21.9213
0.4	21.7568	17.7243	35.9036	27.5496	40.864	30.3903
0.5	31.0519	25.2966	49.3085	37.8354	55.5054	41.2791
0.6	42.4126	34.5516	65.6921	50.4069	73.4004	54.5875
0.7	55.8388	45.4894	85.0547	65.2642	94.5491	70.3157
0.8	71.3306	58.1099	107.4	82.4072	118.95	88.4636
0.9	88.888	72.4131	132.72	101.8359	146.61	109.0312
1	108.51	88.399	161.02	123.5504	177.52	132.0185
1.1	130.2	106.0677	192.29	147.5506	211.68	157.4255
1.2	153.95	125.4192	226.55	173.8365	249.1	185.2523
1.3	179.77	146.4533	263.79	202.4082	289.77	215.4988
1.4	207.66	169.1702	304.14	233.2656	333.69	248.165
1.5	237.61	193.5698	347.19	266.4088	380.87	283.2509
1.6	269.63	219.6522	393.37	301.8376	431.3	320.7565
1.7	303.71	247.4173	442.52	339.5522	484.99	360.6818
1.8	339.86	276.8651	494.65	379.5526	541.93	403.0269
1.9	378.07	307.9957	549.76	421.8386	602.12	447.7917
2	418.35	340.8089	607.84	466.4104	665.56	494.9762

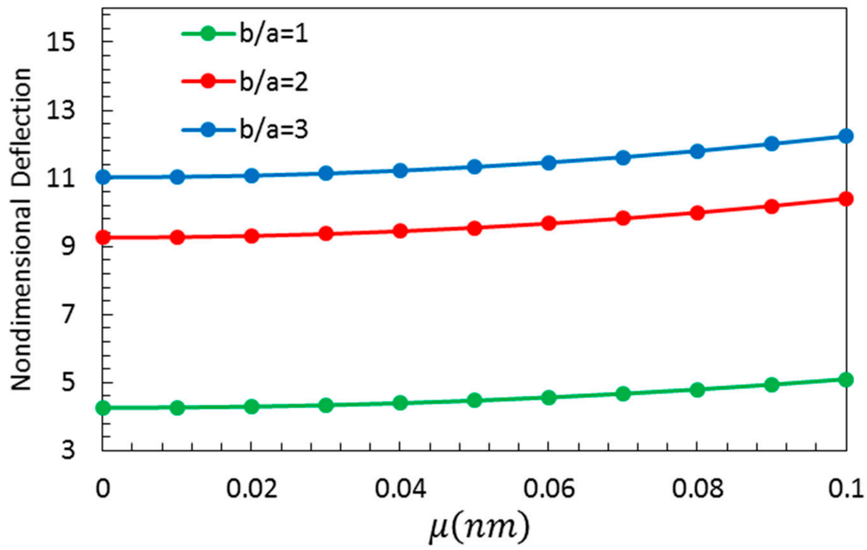

Figure 8. Effect of the nonlocal parameter and b/a ratio on the deflection of deep spherical panels under a uniform load. $R_1 = R_2, R/a = 5, a/h = 10$.

A further parametric investigation considers the combined sensitivity of the deflection response to the nonlocal parameter and Poisson's ratio for a thick deep spherical panel with $a/h = 5$ under a uniform loading condition. As observed in Figure 9, by increasing the nonlocal parameter, the non-dimensional deflection of the deep spherical panel is increased for each value of Poisson's ratio. Moreover, by increasing the Poisson's ratio, the non-dimensional deflection of the deep spherical panel is gradually decreased.

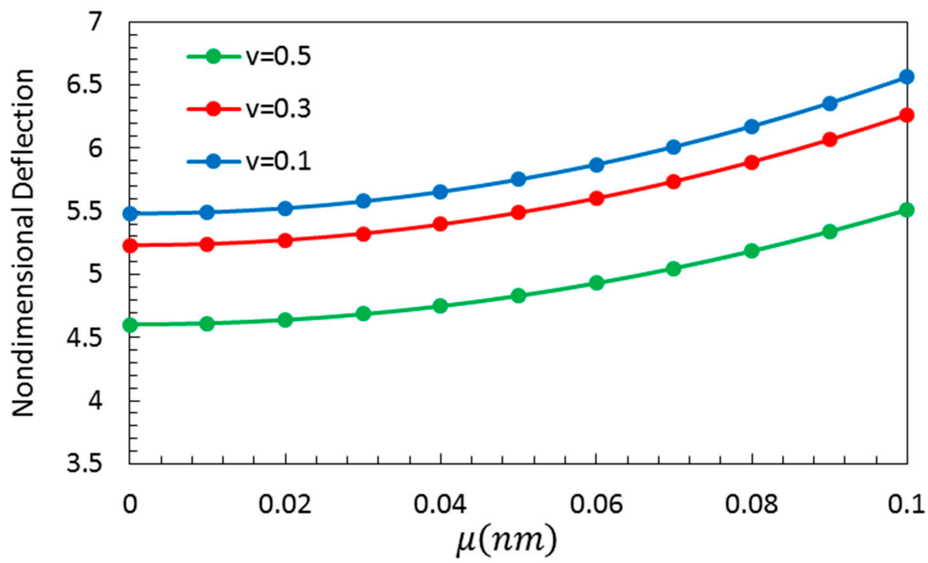

Figure 9. Effect of the nonlocal parameter and Poisson's coefficient on the deflection of deep spherical panels under a uniform load. $R_1 = R_2, R/a = 5, a/h = 5$.

In the histograms of Figure 10, we quantify the effect of the nonlocal parameter and side-to-thickness ratio, a/h, on the deflection ratio of the deep spherical panel under a uniform load. Based on Figure 10, please note that the side-to-thickness ratio does not significantly affect the deflection ratio of the deep spherical panel, independently of the nonlocal parameter, where the only variation in deformability is related to the nonlocal parameter. This justifies the necessity of applying a nonlocal theory instead of the classical elastic ones, which could underestimate the deformability of a nanostructure, in agreement with findings from References [12–14].

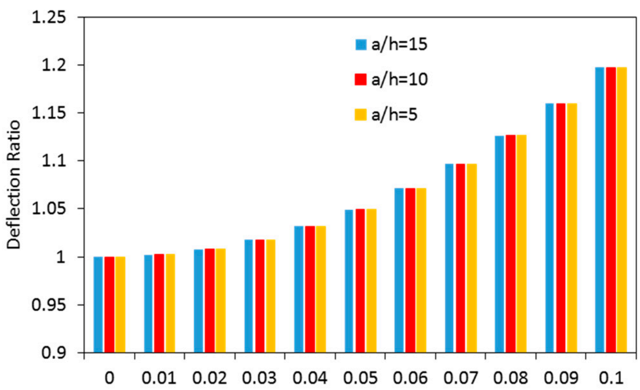

Figure 10. Effect of the nonlocal parameter and a/h ratio on the deflection ratio of deep spherical panels under a uniform load. $R_1 = R_2, R/a = 5$.

5. Conclusions

In the present work, we propose a novel nonlocal shear deformation theory to study the bending deflection of isotropic doubly-curved deep nanoshells. The Hamilton's principle is applied to derive the equations of motion, whose solution is determined by means of the Navier method. The proposed formulation is able to handle both thin and thick, shallow and deep nanoshells within a unified framework. A large parametric investigation is performed systematically to check for the sensitivity of the deflection response for the nonlocal, mechanical, and geometrical parameters, where the following concluding remarks can be summarized.

- An increased nonlocal parameter decreases the stiffness of the isotropic shallow and deep panels, along with a decreased natural frequency, an increased deflection of the nanostructure, and increased stress components.
- An increased value for the side-to-thickness ratio, Poisson's ratio, and length-to-side ratio yields a reduced deflection in the isotropic shallow and deep panel.
- The side-to-thickness ratio does not significantly affect the deflection ratio of shallow and deep panels.
- The axial and longitudinal shear stress components at the top and bottom sides of shallow panels feature higher values than the deep ones.
- Shallow panels are more flexible than deep panels, as visible from their higher deformable response, when compared to deep panels.

Author Contributions: Conceptualization, M.H.D., L.L., R.D. and F.T.; Formal analysis, M.H.D., L.L., R.D. and F.T.; Investigation, M.H.D., L.L. and F.T.; Validation, M.H.D., R.D. and F.T.; Writing—Original Draft, M.H.D., L.L., R.D. and F.T.; Writing—Review & Editing, R.D. and F.T.

Funding: This research received no external funding.

Conflicts of Interest: The authors declare no conflict of interest.

Appendix A

An explicit definition of parameters in Equation 15(a)–(e) is given below

$$\left(A_4, A_5, A_6, A_7, A_8, A_9, A_{10}\right) = \int_{-\frac{h}{2}}^{\frac{h}{2}} Q_{11}\left(1, \xi_3, \xi_3^2, \xi_3^3, f, f\xi_3, f^2\right) d\xi_3$$

$$\left(B_4, \mathrm{B}_5, \mathrm{B}_6, \mathrm{B}_7, \mathrm{B}_8, \mathrm{B}_9, \mathrm{B}_{10}\right) = \int_{-\frac{h}{2}}^{\frac{h}{2}} Q_{12}\left(1, \xi_3, \xi_3^2, \xi_3^3, f, f\xi_3, f^2\right) d\xi_3$$

$$\left(C_4, \mathrm{C}_5, \mathrm{C}_6, \mathrm{C}_7, \mathrm{C}_8, \mathrm{C}_9, \mathrm{C}_{10}\right) = \int_{-\frac{h}{2}}^{\frac{h}{2}} Q_{22}\left(1, \xi_3, \xi_3^2, \xi_3^3, f, f\xi_3, f^2\right) d\xi_3$$

$$\left(D_4, \mathrm{D}_5, \mathrm{D}_6, \mathrm{D}_7, \mathrm{D}_8, \mathrm{D}_9, \mathrm{D}_{10}\right) = \int_{-\frac{h}{2}}^{\frac{h}{2}} Q_{66}\left(1, \xi_3, \xi_3^2, \xi_3^3, f, f\xi_3, f^2\right) d\xi_3$$

$$\left(A_{11}, A_{13}, A_{15}, A_{16}, A_{17}\right) = \int_{-\frac{h}{2}}^{\frac{h}{2}} Q_{11}\left(1+\frac{\xi_3}{R_1}\right)\left(1, \left(1+\frac{\xi_3}{R_1}\right), \left(1+\frac{\xi_3}{R_2}\right), \xi_3, f\right) d\xi_3$$

$$\left(A_{12}, A_{14}, A_{18}, A_{19}\right) = \int_{-\frac{h}{2}}^{\frac{h}{2}} Q_{11}\left(1+\frac{\xi_3}{R_2}\right)\left(1, \left(1+\frac{\xi_3}{R_2}\right), \xi_3, f\right) d\xi_3$$

$$\left(B_{11}, \mathrm{B}_{13}, \mathrm{B}_{15}, \mathrm{B}_{16}, \mathrm{B}_{17}\right) = \int_{-\frac{h}{2}}^{\frac{h}{2}} Q_{12}\left(1+\frac{\xi_3}{R_1}\right)\left(1, \left(1+\frac{\xi_3}{R_1}\right), \left(1+\frac{\xi_3}{R_2}\right), \xi_3, f\right) d\xi_3$$

$$\left(B_{12}, \mathrm{B}_{14}, \mathrm{B}_{18}, \mathrm{B}_{19}\right) = \int_{-\frac{h}{2}}^{\frac{h}{2}} Q_{12}\left(1+\frac{\xi_3}{R_2}\right)\left(1, \left(1+\frac{\xi_3}{R_2}\right), \xi_3, f\right) d\xi_3$$

$$\left(C_{11}, \mathrm{C}_{13}, \mathrm{C}_{15}, \mathrm{C}_{16}, \mathrm{C}_{17}\right) = \int_{-\frac{h}{2}}^{\frac{h}{2}} Q_{22}\left(1+\frac{\xi_3}{R_1}\right)\left(1, \left(1+\frac{\xi_3}{R_1}\right), \left(1+\frac{\xi_3}{R_2}\right), \xi_3, f\right) d\xi_3$$

$$\left(C_{12}, \mathrm{C}_{14}, \mathrm{C}_{18}, \mathrm{C}_{19}\right) = \int_{-\frac{h}{2}}^{\frac{h}{2}} Q_{22}\left(1+\frac{\xi_3}{R_2}\right)\left(1, \left(1+\frac{\xi_3}{R_2}\right), \xi_3, f\right) d\xi_3$$

$$\left(D_{11}, \mathrm{D}_{13}, \mathrm{D}_{15}, \mathrm{D}_{16}, \mathrm{D}_{17}\right) = \int_{-\frac{h}{2}}^{\frac{h}{2}} Q_{66}\left(1+\frac{\xi_3}{R_1}\right)\left(1, \left(1+\frac{\xi_3}{R_1}\right), \left(1+\frac{\xi_3}{R_2}\right), \xi_3, f\right) d\xi_3$$

$$\left(D_{12}, \mathrm{D}_{14}, \mathrm{D}_{18}, \mathrm{D}_{19}\right) = \int_{-\frac{h}{2}}^{\frac{h}{2}} Q_{66}\left(1+\frac{\xi_3}{R_2}\right)\left(1, \left(1+\frac{\xi_3}{R_2}\right), \xi_3, f\right) d\xi_3$$

$$\left(G_{11}, \mathrm{G}_{12}, \mathrm{G}_{13}, \mathrm{G}_{14}\right) = \int_{-\frac{h}{2}}^{\frac{h}{2}} Q_{55}\left(1+\frac{\xi_3}{R_1}\right)^2\left(1, \mathrm{f}, \frac{df}{d\xi_3}, \left(\frac{df}{d\xi_3}\right)^2\right) d\xi_3$$

$$\left(F_{11}, \mathrm{F}_{12}, \mathrm{F}_{13}, \mathrm{F}_{14}\right) = \int_{-\frac{h}{2}}^{\frac{h}{2}} Q_{44}\left(1+\frac{\xi_3}{R_1}\right)^2\left(1, \mathrm{f}, \frac{df}{d\xi_3}, \left(\frac{df}{d\xi_3}\right)^2\right) d\xi_3$$

Appendix B

By substituting Equation (17) into Equation 15(a)–(e), the stiffness matrix is defined as follows

$$K(1,1) = -A_{13}\alpha^2 - D_{13}\beta^2 - \frac{G_{11}}{R_1^2}$$
$$K(1,2) = -B_{15}\alpha\beta - D_{15}\alpha\beta$$
$$K(1,3) = A_{16}\alpha^3 + B_{16}\alpha\beta^2 + 2D_{16}\alpha\beta^2 + \frac{A_{11}\alpha}{R_1} + \frac{B_{11}\alpha}{R_2}$$
$$K(1,4) = -A_{16}y^*\alpha^2 - A_{17}\alpha^2 - D_{16}y^*\beta^2 - D_{17}\beta^2 - \frac{G_{13}}{R_1}$$
$$K(1,5) = -B_{16}y^*\alpha\beta - B_{17}\alpha\beta - D_{16}y^*\alpha\beta - D_{17}\alpha\beta$$
$$K(2,1) = -B_{15}\alpha\beta - D_{13}\alpha\beta$$
$$K(2,2) = -C_{14}\beta^2 - D_{15}\alpha^2 - \frac{F_{11}}{R_2^2}$$
$$K(2,3) = B_{18}\alpha^2\beta + B_{12}\frac{\beta}{R_1} + C_{18}\beta^3 + \frac{C_{12}\beta}{R_2} + 2D_{16}\alpha^2\beta$$
$$K(2,4) = -B_{18}y^*\alpha\beta - B_{19}\alpha\beta - D_{17}\alpha\beta - D_{16}y^*\alpha\beta$$
$$K(2,5) = -C_{18}y^*\beta^2 - C_{19}\beta^2 - D_{16}y^*\alpha^2 - D_{17}\alpha^2 - F_{11}\frac{y^*}{R_2} - \frac{F_{13}}{R_2}$$
$$K(3,1) = A_{16}\alpha^3 + B_{16}\alpha\beta^2 + 2D_{16}\alpha\beta^2 + \frac{A_{11}\alpha}{R_1} + \frac{B_{11}\alpha}{R_2}$$
$$K(3,2) = B_{18}\alpha^2\beta + C_{18}\beta^3 + 2D_{18}\alpha^2\beta + \frac{B_{12}\beta}{R_1} + \frac{C_{12}\beta}{R_2}$$
$$K(3,3) = -A_6\alpha^4 - \frac{A_5\alpha^2}{R_1} - 2B_6\alpha^2\beta^2 - \frac{B_5\alpha^2}{R_2} - \frac{B_5\beta^2}{R_1} - C_6\beta^4 - \frac{C_5\beta^2}{R_2} - 4D_6\alpha^2\beta^2 - \frac{A_5\alpha^2}{R_1} - \frac{A_4}{R_1^2} - \frac{B_5\beta^2}{R_1} +$$
$$-\frac{B_4}{R_1R_2} - \frac{B_5\alpha^2}{R_2} - \frac{B_4}{R_1R_2} - \frac{C_5\beta^2}{R_2} - \frac{C_4}{R_2^2}$$
$$K(3,4) = A_6y^*\alpha^3 + A_9\alpha^3 + B_6y^*\alpha\beta^2 + B_9\alpha\beta^2 + 2D_6y^*\alpha\beta^2 + 2D_9\alpha\beta^2 + A_5y^*\frac{\alpha}{R_1} + A_8\frac{\alpha}{R_1} + B_5y^*\frac{\alpha}{R_2} + B_8\frac{\alpha}{R_2}$$
$$K(3,5) = B_6y^*\alpha^2\beta + B_9\alpha^2\beta + C_6y^*\beta^3 + C_9\beta^3 + 2D_6y^*\alpha^2\beta + 2D_9\alpha^2\beta + B_5y^*\frac{\beta}{R_1} + B_8\frac{\beta}{R_1} + C_5y^*\frac{\beta}{R_2} + C_8\frac{\beta}{R_2}$$

$$K(4,1) = -A_{16}y^*\alpha^2 - D_{16}y^*\alpha^2 - A_{17}\alpha^2 - D_{17}\alpha^2 - G_{11}\frac{y^*}{R_1} - \frac{G_{13}}{R_1}$$
$$K(4,2) = -B_{18}y^*\alpha\beta - D_{18}y^*\alpha\beta - B_{19}\alpha\beta - D_{19}\alpha\beta$$
$$K(4,3) = A_6y^*\alpha^3 + A_5\frac{y^*\alpha}{R_1} + B_6y^*\alpha\beta^2 + B_5\frac{y^*\alpha}{R_2} + 2D_6y^*\alpha\beta^2 + A_9\alpha^3 + A_8\frac{\alpha}{R_1} + B_9\alpha\beta^2 + B_8\frac{\alpha}{R_2} + 2D_9\alpha\beta^2$$
$$K(4,4) = -A_6y^{*2}\alpha^2 - A_9y^*\alpha^2 - D_6y^{*2}\beta^2 - D_9y^*\beta^2 - A_9y^*\alpha^2 - A_{10}\alpha^2 - D_9y^*\beta^2 - D_{10}\beta^2 - G_{11}y^{*2} - G_{13}y^*$$
$$K(4,5) = -B_6y^{*2}\alpha\beta - B_9y^*\alpha\beta - D_6y^{*2}\beta\alpha - D_9y^*\beta\alpha - B_9y^*\alpha\beta - B_{10}\alpha\beta - D_9y^*\alpha\beta - D_{10}\alpha\beta$$
$$K(5,1) = -B_{16}y^*\alpha\beta - D_{16}y^*\alpha\beta - B_{17}\alpha\beta - D_{17}\alpha\beta$$
$$K(5,2) = -C_{18}y^*\beta^2 - D_{18}y^*\alpha^2 - C_{19}\beta^2 - D_{19}\alpha^2 - F_{11}\frac{y^*}{R_2} - \frac{F_{13}}{R_2}$$
$$K(5,3) = B_6y^*\alpha^2\beta + B_5\frac{y^*\beta}{R_1} + C_6y^*\beta^3 + C_5\frac{y^*\beta}{R_2} + 2D_6y^*\alpha^2\beta + B_9\alpha^2\beta + B_8\frac{\beta}{R_1} + C_9\beta^3 + C_8\frac{\beta}{R_2} + 2D_9\alpha^2\beta$$
$$K(5,4) = -B_6y^{*2}\alpha\beta - B_9y^*\alpha\beta - D_6y^{*2}\alpha\beta - D_9y^*\alpha\beta - B_9y^*\alpha\beta - B_{10}\alpha\beta - D_9y^*\alpha\beta - D_{10}\alpha\beta$$
$$K(5,5) = -C_6y^{*2}\beta^2 - C_9y^*\beta^2 - D_6y^{*2}\alpha^2 - D_9y^*\alpha^2 - C_9y^*\beta^2 - C_{10}\beta^2 - D_9y^*\alpha^2 - D_{10}\alpha^2 - F_{11}y^{*^2} - 2F_{13}\,y^* - F_{14}$$

References

1. Love, A.H. *A Treatise on the Mathematical Theory of Elasticity*; Cambridge University Press: Cambridge, UK, 1944; Volume 1, p. 952.
2. Sokolnikoff, I.S.; Walker, M. Tensor analysis: theory and applications. *Am. J. Phys.* **1952**, *20*, 249–250.
3. Sokolnikoff, I.S. *Mathematical Theory of Elasticity*; McGraw-Hill: New York, NY, USA, 1956; Volume 83.
4. Timoshenko, S.P.; Woinowsky-Krieger, S. *Theory of Plates and Shells*; McGraw-Hill: New York, NY, USA, 1959.
5. Leissa, A.W. *Vibration of Shells*; NASA, Washington, United States, 1973.

6. Niordson, F., *Shell theory*, *North-Holland*; Amsterdam, 1985.
7. Tornabene, F.; Fantuzzi, N. *Mechanics of Laminated Composite Doubly-Curvel Shell Structures: The Generalized Differential Quadrature Method and the Strong Formulation Finite Element Method*; Società Editrice Esculapio, Bologna, 2014.
8. Carrera, E. Multilayered shell theories accounting for layerwise mixed description, Part 1: Governing equations. *AIAA J.* **1999**, *37*, 1107–1116.
9. Carrera, E. Historical review of zig-Zag theories for multilayered plates and shells. *Appl. Mech. Rev.* **2003**, *56*, 287–308.
10. Tornabene, F.; Viola, E.; Inman, D.J. 2-D differential quadrature solution for vibration analysis of functionally graded conical, cylindrical shell and annular plate structures. *J. Sound Vib.* **2009**, *328*, 259–290.
11. Duc, N.D.; Quan, T.Q. Transient responses of functionally graded double curved shallow shells with temperature-Dependent material properties in thermal environment. *Eur. J. Mech.-A/Solids* **2014**, *47*, 101–123.
12. Eringen, A.C. Nonlocal polar elastic continua. *Int. J. Eng. Sci.* **1972**, *10*, 1–16.
13. Eringen, A.C. On differential equations of nonlocal elasticity and solutions of screw dislocation and surface waves. *J. Appl. Phys.* **1983**, *54*, 4703–4710.
14. Eringen, A.C. *Nonlocal Continuum Field Theories*; Springer Science & Business Media, New York, 2002.
15. Ramirez, F.; Heyliger, P.R.; Pan, E. Static analysis of functionally graded elastic anisotropic plates using a discrete layer approach. *Compos. Part B Eng.* **2006**, *37*, 10–20.
16. Merdaci, S.; Belghoul, H. High-Order shear theory for static analysis of functionally graded plates with porosities. *Comptes Rendus Mécanique* **2019**, *347*, 207–217.
17. Alibeigloo, A.; Nouri, V. Static analysis of functionally graded cylindrical shell with piezoelectric layers using differential quadrature method. *Compos. Struct.* **2010**, *92*, 1775–1785.
18. Kumar, R.; Mishra, B.; Jain, S. Static and dynamic analysis of smart cylindrical shell. *Finite Elem. Anal. Des.* **2008**, *45*, 13–24.
19. Frikha, A.; Dammak, F. Geometrically non-Linear static analysis of functionally graded material shells with a discrete double directors shell element. *Comput. Methods Appl. Mech. Eng.* **2017**, *315*, 1–24.
20. Mantari, J.L.; Oktem, A.S.; Soares, C.G. Static and dynamic analysis of laminated composite and sandwich plates and shells by using a new higher-Order shear deformation theory. *Compos. Struct.* **2011**, *94*, 37–49.
21. Sahmani, S.; Aghdam, M. Nonlinear instability of hydrostatic pressurized hybrid FGM exponential shear deformable nanoshells based on nonlocal continuum elasticity. *Compos. Part B Eng.* **2017**, *114*, 404–417.
22. Zeighampour, H.; Beni, Y.T.; Karimipour, I. Torsional vibration and static analysis of the cylindrical shell based on strain gradient theory. *Arab. J. Sci. Eng.* **2016**, *41*, 1713–1722.
23. Sahmani, S.; Aghdam, M. Size dependency in axial postbuckling behavior of hybrid FGM exponential shear deformable nanoshells based on the nonlocal elasticity theory. *Compos. Struct.* **2017**, *166*, 104–113.
24. Ke, L.; Wang, Y.; Reddy, J. Thermo-Electro-Mechanical vibration of size-Dependent piezoelectric cylindrical nanoshells under various boundary conditions. *Compos. Struct.* **2014**, *116*, 626–636.
25. Salehipour, H.; Shahsavar, A.; Civalek, O. Free vibration and static deflection analysis of functionally graded and porous micro/nanoshells with clamped and simply supported edges. *Compos. Struct.* **2019**, *221*, 110842.
26. Zeng, S.; Wang, B.; Wang, K. Static stability analysis of nanoscale piezoelectric shells with flexoelectric effect based on couple stress theory. *Microsyst. Technol.* **2018**, *24*, 2957–2967.
27. Arefi, M.; Mohammad-Rezaei Bidgoli, E.; Dimitri, R.; Tornabene, F. Free vibrations of functionally graded polymer composite nanoplates reinforced with graphene nanoplatelets. *Aerosp. Sci. Technol.* **2018**, *81*, 108–117.
28. Jouneghani, F.Z.; Dimitri, R.; Tornabene, F. Structural response of porous FG nanobeams under hygro-Thermo-Mechanical loadings. *Compos. Part B Eng.* **2018**, *152*, 71–78.
29. Arefi, M.; Mohammad-Rezaei Bidgoli, E.; Dimitri, R.; Bacciocchi, M.; Tornabene, F. Nonlocal bending analysis of curved nanobeams reinforced by graphene nanoplatelets. *Compos. Part B Eng.* **2019**, *166*, 1–12.
30. Arefi, M.; Bidgoli, E.M.-R.; Dimitri, R.; Tornabene, F.; Reddy, J.N. Size-Dependent free vibrations of FG polymer composite curved nanobeams reinforced with graphene nanoplatelets resting on Pasternak foundations. *Appl. Sci.* **2019**, *9*, 1580.
31. Karami, B.; Janghorban, M.; Shahsavari, D.; Dimitri, R.; Tornabene, F. Nonlocal Buckling Analysis of Composite Curved Beams Reinforced with Functionally Graded Carbon Nanotubes. *Molecules* **2019**, *24*, 2750.

32. Malikan, M.; Nguyen, V.B.; Dimitri, R.; Tornabene, F. Dynamic modeling of non-Cylindrical curved viscoelastic single-Walled carbon nanotubes based on the second gradient theory. *Mater. Res. Express* **2019**, *6*, 075041.
33. Arefi, M. Analysis of a doubly curved piezoelectric nano shell: nonlocal electro-Elastic bending solution. *Eur. J. Mech.-A/Solids* **2018**, *70*, 226–237.
34. Tornabene, F.; Fantuzzi, N.; Viola, E.; Carrera, E. Static analysis of doubly-Curved anisotropic shells and panels using CUF approach, differential geometry and differential quadrature method. *Compos. Struct.* **2014**, *107*, 675–697.
35. Tornabene, F.; Viola, E. Static analysis of functionally graded doubly-Curved shells and panels of revolution. *Meccanica* **2013**, *48*, 901–930.
36. Viola, E.; Tornabene, F.; Fantuzzi, N. Static analysis of completely doubly-Curved laminated shells and panels using general higher-Order shear deformation theories. *Compos. Struct.* **2013**, *101*, 59–93.
37. Liew, K.; Lim, C. A higher-Order theory for vibration of doubly curved shallow shells. *J. Appl. Mech.* **1996**, *63*, 587–593.
38. Amabili, M.; Reddy, J. A new non-Linear higher-Order shear deformation theory for large-Amplitude vibrations of laminated doubly curved shells. *Int. J. Non-Linear Mech.* **2010**, *45*, 409–418.
39. Jouneghani, F.Z.; Dashtaki, P.M.; Dimitri, R.; Bacciocchi, M.; Tornabene, F. First-Order shear deformation theory for orthotropic doubly-Curved shells based on a modified couple stress elasticity. *Aerosp. Sci. Technol.* **2018**, *73*, 129–147.
40. Arefi, M.; Rabczuk, T. A nonlocal higher order shear deformation theory for electro-Elastic analysis of a piezoelectric doubly curved nano shell. *Compos. Part B Eng.* **2019**, *168*, 496–510.
41. Karami, B.; Janghorban, M.; Tounsi, A. Variational approach for wave dispersion in anisotropic doubly-Curved nanoshells based on a new nonlocal strain gradient higher order shell theory. *Thin-Walled Struct.* **2018**, *129*, 251–264.
42. Dindarloo, M.H.; Li, L. Vibration analysis of carbon nanotubes reinforced isotropic doubly-Curved nanoshells using nonlocal elasticity theory based on a new higher order shear deformation theory. *Compos. Part B Eng.* **2019**, *175*, 107170.
43. Karami, B.; Shahsavari, D.; Janghorban, M. On the dynamics of porous doubly-Curved nanoshells. *Int. J. Eng. Sci.* **2019**, *143*, 39–55.
44. Chaudhuri, R.A.; Kabir, H.R. On analytical solutions to boundary-Value problems of doubly-Curved moderately-Thick orthotropic shells. *Int. J. Eng. Sci.* **1989**, *27*, 1325–1336.
45. Tornabene, F.; Fantuzzi, N.; Bacciocchi, M. On the mechanics of laminated doubly-Curved shells subjected to point and line loads. *Int. J. Eng. Sci.* **2016**, *109*, 115–164.
46. Ghayesh, M.H.; Farokhi, H. Nonlinear mechanics of doubly curved shallow microshells. *Int. J. Eng. Sci.* **2017**, *119*, 288–304.
47. Zaoui, F.Z.; Ouinas, D.; Tounsi, A. New 2D and quasi-3D shear deformation theories for free vibration of functionally graded plates on elastic foundations. *Compos. Part B Eng.* **2019**, *159*, 231–247.
48. Mantari, J.; Oktem, A.; Soares, C.G. A new higher order shear deformation theory for sandwich and composite laminated plates. *Compos. Part B Eng.* **2012**, *43*, 1489–1499.
49. Reddy, J.N. *Mechanics of Laminated Composite Plates and Shells: Theory and Analysis*; CRC Press, Boca Raton London New York Washimgtpn D.C., 2003.
50. Romano, G.; Barretta, R.; Diaco, M. On nonlocal integral models for elastic nano-Beams. *Int. J. Mech. Sci.* **2017**, *131–132*, 490–499.
51. Barretta, R.; Ali Faghidian, S.; Luciano, R.; Medaglia, C.M.; Penna, R. Free vibrations of FG elastic Timoshenko nano-Beams by strain gradient and stress-Driven nonlocal models. *Compos. Part B Eng.* **2018**, *154*, 20–32.
52. Romano, G.; Luciano, R.; Barretta, R.; Diaco, M. Nonlocal integral elasticity in nanostructures, mixtures, boundary effects and limit behaviours. *Contin. Mechancis Thermodyn.* **2018**, *30*, 641–655.
53. Pinnola, F.P.; Ali Faghidian, S.; Barretta, R.; Marotti de Sciarra, F. Variationally consistent dynamics of nonlocal gradient elastic beams. *Int. J. Eng. Sci.* **2020**, *149*, 103220.
54. Reddy, J.N. A simple higher-Order theory for laminated composite plates. *J. Appl. Mech.* **1984**, *51*, 745–752.
55. Reddy, J.; Liu, C. A higher-Order shear deformation theory of laminated elastic shells. *Int. J. Eng. Sci.* **1985**, *23*, 319–330.

56. Reddy, J.N. *Energy and Variational Methods in Applied Mechanics: With an Introduction to the Finite Element Method*; Wiley: New York, NY, USA, 1984.
57. Reddy, J.N. *An Introduction to the Finite Element Method*; McGraw-Hill Book Company, New York, 1984.
58. Ferreira, A.; Roque, C.; Martins, P. Analysis of composite plates using higher-Order shear deformation theory and a finite point formulation based on the multiquadric radial basis function method. *Compos. Part B Eng.* **2003**, *34*, 627–636.
59. Ferreira, A.; Roque, C.; Jorge, R. Analysis of composite plates by trigonometric shear deformation theory and multiquadrics. *Comput. Struct.* **2005**, *83*, 2225–2237.
60. Xiang, S.; Wang, K.-M.; Sha, Y.-D.; Shi, H. Analysis of isotropic, sandwich and laminated plates by a meshless method and various shear deformation theories. *Compos. Struct.* **2009**, *91*, 31–37.
61. Bhimaraddi, A. Three-Dimensional elasticity solution for static response of orthotropic doubly curved shallow shells on rectangular planform. *Compos. Struct.* **1993**, *24*, 67–77.